Brain, Behavior, and Immunity 123 (2025) 886–902

Contents lists available at ScienceDirect

Brain Behavior and Immunity

journal homepage: www.elsevier.com/locate/ybrbi

Full-length Article

Tumor-derived cyclooxygenase-2 fuels hypothalamic inflammation

Xiaolin Li [a,b], Xinxia Zhu [b], Parham Diba [b,c], Xuan Shi [a], Frank Vrieling [d], Fleur A.C. Jansen [a], Michiel G.J. Balvers [a], Ian de Bus [a], Peter R. Levasseur [b], Ariana Sattler [b,e], Paige C. Arneson-Wissink [f], Mieke Poland [a], Renger F. Witkamp [a], Klaske van Norren [a,*,1], Daniel L. Marks [b,f,g,*,1]

[a] Nutritional Biology, Division of Human Nutrition, Wageningen University, Wageningen, the Netherlands
[b] Papé Family Pediatric Research Institute, Oregon Health & Science University, Portland, OR, USA
[c] Medical Scientist Training Program, Oregon Health & Science University, Portland, OR, USA
[d] Department of Internal Medicine, Radboud University Medical Centre, Nijmegen, the Netherlands
[e] Department of Cell, Developmental & Cancer Biology, Oregon Health & Science University, Portland, OR, USA
[f] Brenden Colson Center for Pancreatic Care, Oregon Health and Science University, Portland, OR, USA
[g] Knight Cancer Institute, Oregon Health & Science University, Portland, OR, USA

A B S T R A C T

Hypothalamic inflammation often coincides with cancer and cachexia-anorexia. Prior work established the significance of tumor-derived inflammatory factors in triggering hypothalamic inflammation, yet the precise mechanisms remained elusive. Here, we demonstrate that prostaglandin E2 (PGE2), produced in the tumor via cyclooxygenase-2 (COX-2), plays a pivotal role in this context. PGE2 itself directly exerts pro-inflammatory effects on the hypothalamus through the EP4 receptor, while also augmenting hypothalamic inflammation via NF-κB pathways in the presence of host gut-derived pathogen-associated molecular patterns (PAMPs). In tumor-bearing mice, we confirm this synergistic interaction between tumor-derived COX-2/PGE2 and host-derived lipopolysaccharide (LPS) in amplifying hypothalamic inflammation. Supporting this mechanism we find that the tumor-specific knockout of COX-2 attenuates hypothalamic inflammation and improves survival in mice. Together, these findings highlight the mechanisms of tumor-associated COX-2 in fuelling hypothalamic inflammation. They also emphasize the potential of tumor-specific COX-2 inhibition and targeting gut permeability as a novel therapeutic strategy for improving clinical outcomes in cancer patients.

1. Introduction

The hypothalamus serves as a master regulator of the body's systemic homeostasis. It plays a pivotal role in regulating the autonomic nervous system and is crucial in the manifestation of sickness behavior. In cancer patients, functional alterations in brain areas that control energy homeostasis contribute to the onset of anorexia, reduced food intake, and increased catabolism in muscle tissue. As a response to cancer-induced systemic inflammation, the hypothalamus initiates the synthesis of pro-inflammatory cytokines. These mediators are known to influence the activity of neuroendocrine circuits (Burfeind et al., 2016a). Previous studies indicate that hypothalamic inflammation plays a key role in initiating and exacerbating cancer-associated muscle loss (Braun et al., 2011). Hypothalamic inflammation activates the hypothalamic–pituitary–adrenal (HPA) axis (Van Norren et al., 2017) by stimulating the release of adrenocorticotropic hormone. This, in turn, enhances the production of glucocorticoids, which contribute to muscle breakdown through the activation of glucocorticoid receptors (Braun et al., 2014). Additionally, inflammation inhibits hypothalamic serotonin production, which, by suppressing excitatory neurons, contributes to fatigue and decreased appetite (Ryan et al., 2007).

Multiple lines of research, including those from our labs, increasingly suggest that the enzyme Cyclooxygenase (COX)-2 plays a crucial role at various stages of cancer (Bell and Zelenay, 2022; Davis et al., 2004; Li et al., 2022). The COX-2 catalyzes the conversion of poly-unsaturated fatty acids, including arachidonic acid, into oxygenated metabolites like prostaglandins and thromboxanes. Among the multiple COX-2-derived prostaglandins, prostaglandin E2 (PGE2) is a prominent pro-inflammatory mediator (Wang and Dubois, 2006) acting through specific G-protein coupled receptors, including EP1, EP2, EP3, and EP4 (Markovič et al., 2017). Elevated COX-2 expression and increased PGE2 production are commonly observed in colon, breast, and pancreatic

* Corresponding authors at: Papé Family Pediatric Research Institute, Oregon Health & Science University, Portland, OR, USA (D.L. Marks). Nutritional Biology, Division of Human Nutrition, Wageningen University, Wageningen, The Netherlands (Klaske van Norren).
E-mail addresses: klaske.vannorren@wur.nl (K. van Norren), dan@endevicabio.com (D.L. Marks).
[1] Contributed equally to this work.

https://doi.org/10.1016/j.bbi.2024.11.002
Received 22 April 2024; Received in revised form 10 October 2024; Accepted 2 November 2024
Available online 4 November 2024

tumors (Wang and Dubois, 2006). Another significant finding is the impaired gut barrier function during cancer, which leads to increased intestinal permeability to macromolecules (Bindels et al., 2018; Li et al., 2022) and bacterial translocation (Klein et al., 2013). This includes the entry of endotoxins such as lipopolysaccharide (LPS) into the bloodstream, which can be sensed by the hypothalamus and induce hypothalamic inflammation (Witkamp and van Norren, 2018). This inflammatory process can be exacerbated by interventions like chemotherapy and radiotherapy (Haroun et al., 2023; Munford, 2016; Roy and Trinchieri, 2017), as well as certain nonsteroidal anti-inflammatory drugs (NSAIDs), which negatively impact intestinal barrier function.

We previously demonstrated (Li et al., 2022) that inflammatory factors originating from the tumor play a critical role in mediating hypothalamic inflammation. Our *in vitro* evidence suggested that tumor-associated COX-2 and PGE2, in conjunction with pathogen-associated molecular patterns (PAMPs), can lead to amplified hypothalamic neuroinflammation. However, the underlying mechanisms remained unclear.

Here, we delve deeper into the metabolic pathways underlying the interplay between tumor-derived COX-2 and hypothalamic inflammation. With *in vitro* studies, we first investigated the PGE2 receptors involved using relevant agonists and antagonists. Looking for the optimal *in vivo* model to study the amplification of hypothalamic inflammation, we selected the orthotopic, syngeneic 4662 mouse model

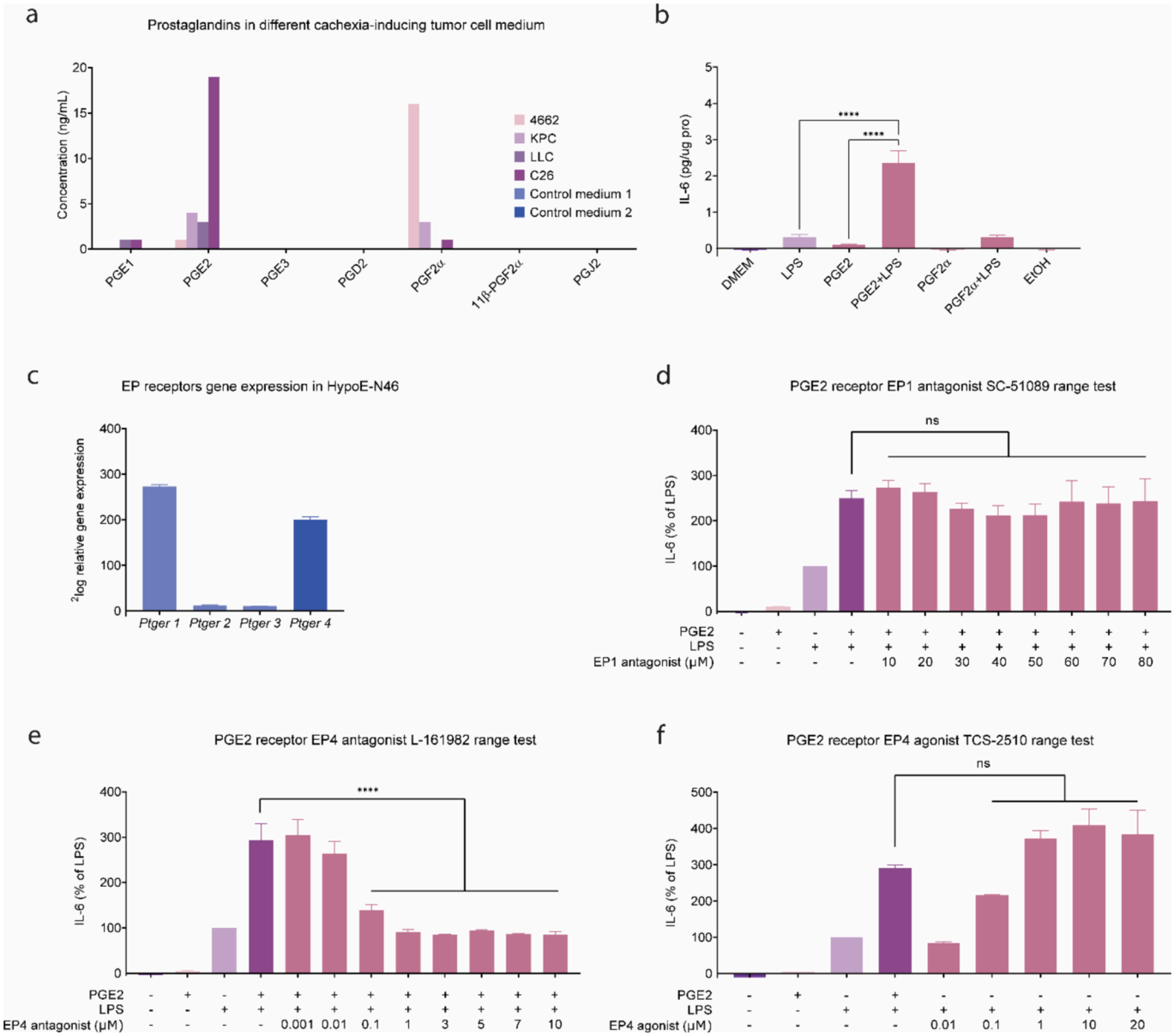

Fig. 1. Tumor-secreted PGE2 enhances hypothalamic inflammation via EP4 receptor. a Prostaglandin levels in the cachexia-inducing tumor cell secretomes (4662, KPC, LLC and C26), measured by UPLC-MS/MS. b IL-6 secretion of HypoE-N46 cells upon exposure to different prostaglandins at a dose of 6500 pg/mL, combined with or without LPS at a dose of 31.6 ng/mL. c Gene expression of PGE2 receptors EP1 (Ptger1), EP2 (Ptger2), EP3 (Ptger3), and EP4 (Ptger4) in HypoE-n46 cells, measured by microarray (Dwarkasing et al., 2016). IL-6 release of HypoE-N46 cells upon exposure to different concentrations of the selective EP antagonists and agonists: d EP1 antagonist SC-51089 (10, 20, 30, 40, 50, 60, 70, 80 μM), e EP4 antagonist L-161982 (0.001, 0.01, 0.1, 1, 3, 5, 7, 10 μM), f EP4 agonist TCS 2510 (0.01, 0.1, 1, 10, 20 μM). HypoE-n46 cells were cultured in fresh DMEM medium for 24 h and then treated with the indicated conditions for 24 h. The media were collected for analysis. Data in a was expressed of N = 1. Data in b, d-f were expressed as mean ± SEM of N = 3 independent experiments with triplicate wells. Data represented in b, d-f were analyzed by one-way ANOVA with Bonferroni's post hoc test, compared to PGE2 + LPS group. Partial significance is labeled to emphasize the highlighted comparisons. *p ≤ 0.05, **p ≤ 0.01, and ***p ≤ 0.001, ****p ≤ 0.0001.

of pancreatic ductal adenocarcinoma (PDAC). This model represents a relatively less aggressive cancer phenotype compared to other mouse models of PDAC (Olson et al., 2021). Notably, the 4662 cell line and corresponding mouse model exhibits lower plasma PGE2 levels and smaller changes in intestinal permeability (Li et al., 2022), compared to the KPC tumor cell line and mouse model from which it originates. Therefore the 4662 mouse model provides a conducive environment for the LPS administration to simulate increased intestinal permeability as present in the KPC model (Li et al., 2022). In light of our previous findings regarding the anti-inflammatory effect of the COX-2 inhibitor celecoxib (Li et al., 2022), we generated CRISPR/Cas9-mediated *Ptgs2* gene knockout in the KPC tumor cells, leveraging the pronounced cachexia syndrome manifested in the KPC mouse model for a comprehensive assessment of the knockout benefits. This multifaceted approach allowed us to explore the cross-talk between the hypothalamus, the tumor, and the intestine in various aspects of cancer, and uncover the role of tumor-specific COX-2 in underlying mechanisms.

2. Results

1. Tumor-secreted PGE2 enhances hypothalamic inflammation via EP4 receptor.

Tumor-secreted PGE2 may play a role in amplifying the influence of gut bacteria-derived LPS on the inflammatory response in the hypothalamus (Li et al., 2022). To explore the mechanism underlying the interactions between PGE2 and LPS at the level of the hypothalamus, we utilized a hypothalamic neuronal cell line (mHypoE-N46/Clu138), originally derived from a male mouse. The cells were exposed to LPS and various prostaglandins. We employed a range of antagonists and agonists to investigate the involvement of various receptors and pathways. Inflammation was assessed by measuring the IL-6 levels in the culture medium secreted by HypoE-N46 cells.

To compare the prostaglandin profile of pancreatic cancer cell line 4662 in the secretome with that of other murine tumor cell lines known to induce cachexia, we conducted an analysis of the media from four different cell lines and observed that each of these cell lines secreted a high amount of PGE2 (Fig. 1a). Of note was that the other pancreatic cancer cell line, KPC, apparently produced more PGE2 than the 4662 cell line (medium concentrations 3.915 ng/mL vs 1.358 ng/mL). This is consistent with our earlier observations that KPC tumor-bearing mice presented a more aggressive cancer phenotype than 4662 tumor-bearing mice. In addition, a higher concentration of PGF2α was also observed in these two secretomes. Subsequently, we incubated HypoE-N46 cells with both LPS and various prostaglandins to investigate their combined effects. In line with our previous studies (Li et al., 2022), PGE2 enhanced the secretion of LPS-induced IL-6 in the HypoE-N46 cells. By contrast, the addition of PGF2α did not increase IL-6 secretion (Fig. 1b).

Four membrane receptor subtypes that can bind to PGE2 are distinguished based on their genomic and pharmacological characteristics. Their relative affinity for PGE2 is EP3 > EP4 > EP2 > EP1 (Karpisheh et al., 2020). To identify the most relevant EP in this context and its associated signal transduction pathways, we first explored the gene expression of PGE2 receptors in HypoE-N46 cells. Genes coding for EP1 (*Ptger1*) and EP4 (*Ptger4*) were expressed at relatively high levels compared to those for EP2 (*Ptger2*) and EP3 (*Ptger3*) (Fig. 1c).

Next to that, we incubated HypoE-N46 cells with known antagonists of the four receptors and measured their effects on IL-6 release. Co-incubation with EP1 antagonist (SC-51089) at concentrations up to 80 μM did not diminish the effects of PGE2 (Fig. 1d). By contrast, the EP4 antagonist (L-161982) blocked the effects of PGE2 at a low concentration (0.1 μM; $P < 0.0001$) (Fig. 1e). These suggest that the EP4 receptor is likely involved in the stimulation of the LPS-induced IL-6 secretion via PGE2. To gain more certainty regarding the potential involvement of the EP4 receptor, we conducted additional experiments using a specific EP4 agonist (TCS2510) in combination with LPS stimulation. The EP4 agonist, at a concentration of 1 μM, increased LPS-induced IL-6 release to a level equivalent to that of PGE2 (Fig. 1f), which further indicates a significant role of the EP4 receptor in mediating LPS-induced hypothalamic IL-6 release through PGE2. Additionally, co-incubation with EP2 antagonist PF-04418948 at concentrations up to 80 μM did not significantly reduce the effects of PGE2 (Supplementary Fig. 2a). When the EP3 antagonist L-798106 was added at a concentration of 40 μM, PGE2 was no longer able to significantly increase LPS-induced IL6 release (Supplementary Fig. 2b). Given that this concentration of L-798106 is much higher than its Ki value for the EP3 receptor (0.3 nM, compared to 916, >5000, and > 5000 nM for EP4, EP1, and EP2, respectively), it is likely that loss of selectivity may be a factor. The EP3 agonist sulprostone at concentrations up to 20 μM did not enhance an LPS-induced inflammatory response to the extent as PGE2 (Supplementary Fig. 2c). These findings suggest that EP2 and EP3 are not directly involved in amplifying the inflammatory response.

Given that the HypoE-N46 cell line employed in this study is of neuronal origin, we aimed to investigate the extent to which PGE2 receptors were present in different cell types of the hypothalamus. To achieve this, we re-analyzed single-cell RNA sequencing data from the arcuate nucleus of the hypothalamus including 20,921 publicly available single-cell transcriptomes (Campbell et al., 2017). We found that EP4 (*Ptger4*) mRNA was expressed centrally in neurons1 (Supplementary Fig. 1), consistent with the results obtained with HypoE-N46 cells, confirming that EP4 was predominantly expressed in HypoE-N46 cells.

2. Interactions of PGE2/EP4 with PAMPs/TLR activate inflammatory signaling via NF-κB.

Given that excessive inflammation in cancer arises from both the tumor and the host, once we validated the receptor EP4 in the hypothalamus activated by tumor-derived PGE2, we delved into exploring the TLR pathway activated by host intestine-derived PAMPs. This aimed to elucidate the potential mechanisms involved in the crosstalk between the tumor, gut, and hypothalamic neuro-inflammation.

The LPS is a ligand for Toll-like receptor 4 (TLR4). Stimulation of TLR4 initiates a bifurcated pathway: 1) the MyD88-dependent pathway that mediates proinflammatory cytokine activation, and 2) the MyD88-independent pathway that promotes Type I interferon genes (Lu et al., 2008). Downstream signaling through the MyD88-dependent pathway involves molecules like NF-κB and CREB, ultimately resulting in the production of proinflammatory cytokines including IL-6 (Swanson et al., 2020).

Various inhibitors were used to corroborate the involvement of the TLR4 pathway in HypoE-N46 cells. The IL-6 release was inhibited by the TLR4 inhibitor (TAK-242) at concentrations from 20 to 100 ng/mL (Fig. 2a) and decreased by the NF-κB inhibitor (BMS-345541, 7 μM) (Fig. 2b). However, inhibiting CREB did not yield a decrease in IL-6 release and co-inhibition of CREB and NF-κB did not show additional effects. This data suggests that NF-κB is pivotal in mediating PGE2-induced hypothalamic inflammation.

Toll-like receptor 2/1 (TLR2/1) signaling is another MyD88-dependent response that stimulates the kinase activity of the IRAK complex (Caplan and Maguire-Zeiss, 2018). To further substantiate the involvement of NF-κB from different TLR signaling pathways, we used Pam3Cys-SKKKK (Pam) to activate TLR2/1 (Supplementary Fig. 2d). Similar to LPS, Pam supported PGE2-induced hypothalamic IL-6 release (Supplementary Fig. 2e). The IL-6 release was reduced by 50 % with the TLR2/1 inhibitor (MMG-11) at 10 μM, and also decreased by the NF-κB inhibitor (Supplementary Fig. 2f,g), underscoring the critical roles of TLR2/1 and NF-κB in amplifying hypothalamic IL-6 secretion.

In line with the prevailing notion of multi-therapeutic approaches, we evaluated a combination of targeting both tumor-derived PGE2 and host gut-derived PAMPs pathways to minimize hypothalamic inflammation in cancer.

When LPS and PGE2 were added together, the IL-6 concentration increased up to 304 % compared with LPS alone ($P < 0.0001$) (Fig. 2d). This rise was suppressed by an EP4 antagonist or an NF-κB inhibitor.

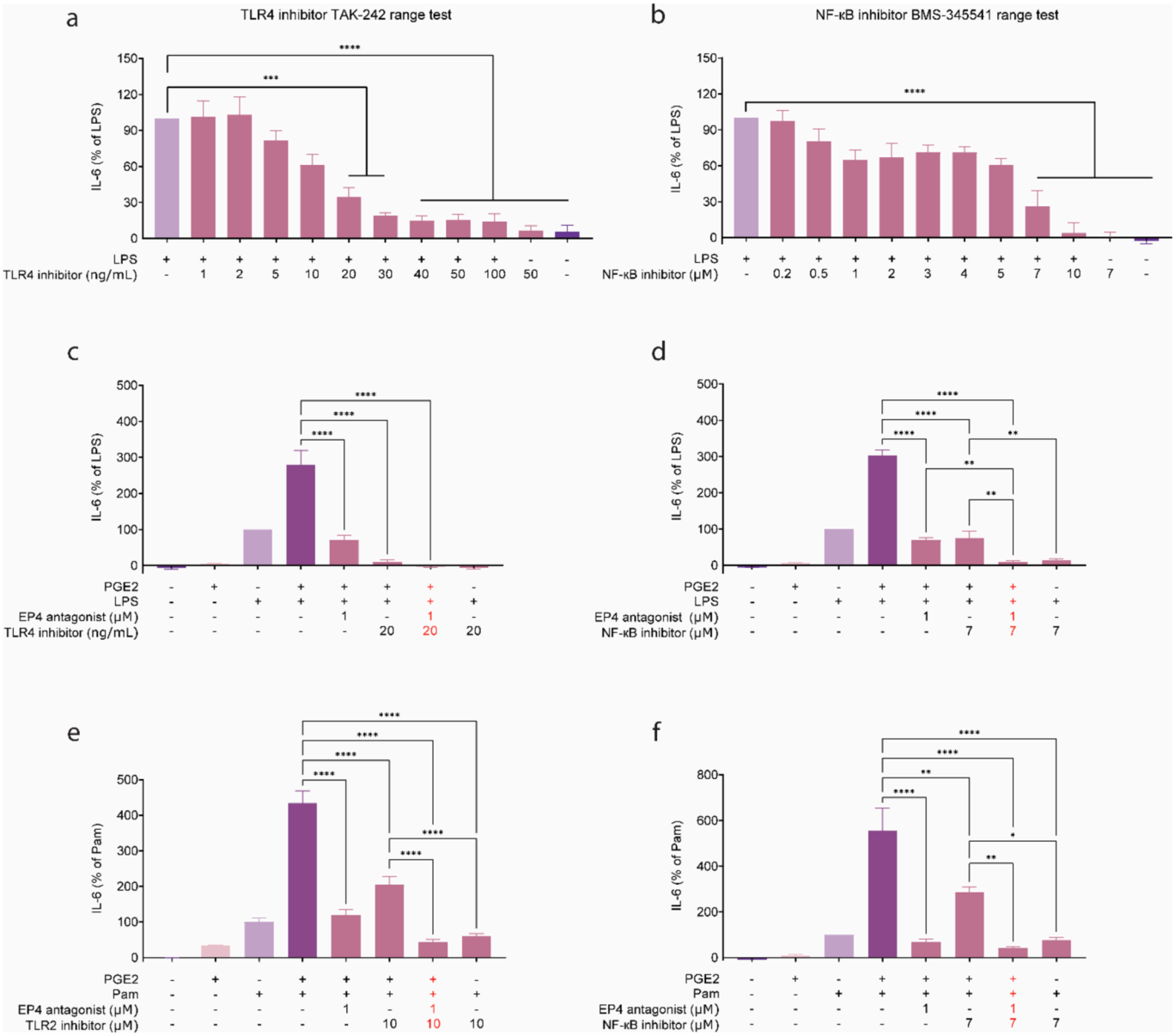

Fig. 2. Interactions of PGE2/EP4 with PAMPs/TLR activate inflammatory signaling via NF-κB. IL-6 release of HypoE-N46 cells upon exposure to: **a** concentration range of TLR4 inhibitor TAK-242 (1 ng/mL to 50 ng/mL) combined with LPS (31.6 ng/mL), **b** concentration range of NF-κB (IκB kinase) inhibitor BMS-345541 (0.2 to 10 μM) combined with LPS (31.6 ng/mL). IL-6 release of HypoE-N46 cells upon exposure to EP4 antagonist L-161,982 (1 uM) and **c** TLR4 inhibitor TAK-242 (20 ng/mL), **d** NF-κB (IκB kinase) inhibitor BMS-345541 (7 uM), combined with PGE2 (6500 pg/mL) and LPS (31.6 ng/mL). IL-6 release of HypoE-N46 cells upon exposure to EP4 antagonist L-161,982 (1 uM) and **e** TLR2 inhibitor MMG-11 (10 μM), **f** NF-κB (IκB kinase) inhibitor BMS-345541 (7 μM), combined with PGE2 (6500 pg/mL) and Pam3CSK4 (TLR2/TLR1 ligand) (10 ng/mL). HypoE-n46 cells were cultured in fresh DMEM medium for 24 h and then treated with the indicated conditions for 24 h. The media were collected for analysis. All data were expressed as mean ± SEM of N = 3 independent experiments with triplicate wells. Data represented in **a** and **b** were analyzed by one-way ANOVA with Bonferroni's post hoc test, compared to LPS group. Data represented in **c-f** were analyzed by one-way ANOVA with Bonferroni's post hoc test. Partial significance is labeled to emphasize the highlighted comparisons. *$p \leq 0.05$, **$p \leq 0.01$, and ***$p \leq 0.001$, ****$p \leq 0.0001$.

When EP4 antagonist and NF-κB inhibitor were administered in combination, IL-6 secretion decreased to 9 % compared with LPS alone ($P < 0.0001$) (Fig. 2d). While the NF-κB inhibitor reduced LPS-induced IL-6 by 14 %, the addition of PGE2 reinstated the inflammatory signal to 76 % (LPS + BMS vs PGE2 + LPS + BMS, $P < 0.01$) (Fig. 2d). Similar to LPS, Pam-induced IL-6 production was decreased to 77 % with the NF-κB inhibitor, but it was reinstated by PGE2 up to 286 % (Pam + BMS vs PGE2 + Pam + BMS, $P < 0.05$) (Fig. 2f), underscoring potent amplifying effects of PGE2. Notably, PGE2 was unable to increase BMS-inhibited IL-6 production when combined with the EP4 inhibitor, highlighting the relevance of co-suppressing both EP4- and NF-κB- mediated signaling. Furthermore, pre-incubation with the EP4 antagonist had even more pronounced anti-inflammatory effects. The IL-6 release was significantly decreased to a similar level as the negative control by TLR4 inhibitor (Fig. 2c) and TLR2/1 inhibitor (Fig. 2e) when combined with EP4 antagonist, suggesting that targeting both the EP4 receptor and TLR/NF-κB might offer a promising anti-inflammatory approach in the context of cancer.

3. Hypothalamic inflammation is amplified in tumor-bearing mice in response to LPS.

Consistent with prior research, male and female mice bearing pancreatic 4662 tumors showed a reduction in food consumption compared to the sham control mice (Fig. 3a, Supplementary Fig. 3a). The terminal tumor mass was identical between the male and female

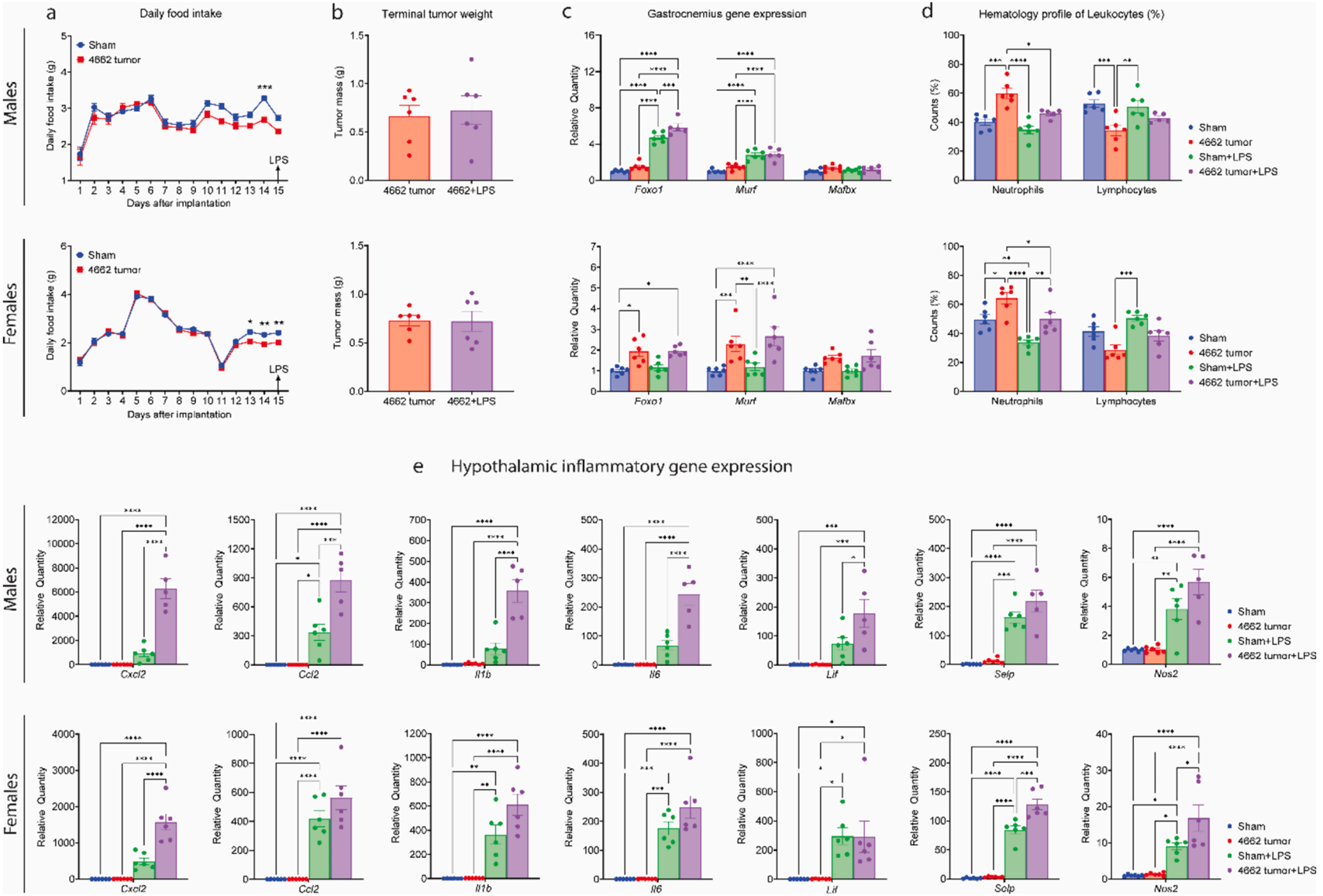

Fig. 3. Hypothalamic inflammation is amplified in tumor-bearing mice in response to LPS. **a** Daily food intake, **b** terminal tumor weight, **c** gastrocnemius gene expression profiles, **d** relative neutrophil and lymphocyte levels in male and female cohorts. **e** RT-PCR analysis of pro-inflammatory transcripts in the hypothalamus (represented as relative quantity to sham control) in male and female cohorts. N = 6 per group except for male 4662 + LPS (N = 5). All data were expressed as mean ± SEM. Data represented in **a, c, d** were analyzed by two-way ANOVA with Bonferroni's post hoc test. **b** Analyzed by two-tailed Student's *t* test. **e** Analyzed by one-way ANOVA with Bonferroni's post hoc test. $*p \leq 0.05$, $**p \leq 0.01$, and $***p \leq 0.001$, $****p \leq 0.0001$. Sham operation controls = blue, 4662 tumor = red, Sham treated with LPS = green, 4662 tumor treated with LPS = purple. (For interpretation of the references to colour in this figure legend, the reader is referred to the web version of this article.)

tumor mice (Fig. 3b). Both groups showed an increase in body weight while maintaining consistent food orts compared to sham controls (Supplementary Fig. 3b,c).

The expression of skeletal muscle catabolic genes, *Mafbx*, *Murf1*, and *Foxo1,* was significantly elevated in the female tumor mice, suggesting cancer-related muscle wasting (Fig. 3c). Moreover, blood neutrophils were significantly higher in both male and female tumor mice, compared to the sham mice, indicating the increased systemic inflammation (Fig. 3d, Supplementary Fig. 3d,e).

At day 15 after tumor implantation, the mice received an intraperitoneal injection of either LPS or saline, and the hypothalami were collected 4 h later. In both sexes of mice, while there was no change in hypothalamic inflammatory gene expression between sham and tumor mice, LPS exposure significantly increased the expression of the most of hypothalamic genes in tumor mice compared to LPS-treated sham mice (Fig. 3e). Particularly, in male tumor mice receiving LPS, the hypothalamic *Cxcl2* expression was seven-fold higher compared to male sham mice receiving LPS ($P < 0.0001$). This high amplification of gene expression was also observed in *Ccl2* (2.6-fold), *Il1b* (10-fold), *Il6* (3.7-fold), and *Lif* (2.5-fold). However, the apparent increase of *Selp* and *Nos2* expression was not significant (Fig. 3e). In female tumor mice receiving LPS, the hypothalamic *Cxcl2* expression was 3.2-fold higher compared to female sham mice receiving LPS ($P < 0.0001$). The expression of other inflammatory genes in female tumor mice receiving LPS appeared slightly increased compared to female sham mice receiving LPS, but this was not significant except for *Nos2* ($P < 0.005$). Additionally, the *Cxcl2* expression levels in female sham mice receiving LPS were half those of male sham mice receiving LPS mice (Fig. 3e). In conclusion, there was marked sensitization in hypothalamic inflammation in tumor-bearing mice upon LPS exposure. Furthermore, LPS exposure elicited a lower response in hypothalamic inflammatory gene expression in female tumor mice compared to male tumor mice, indicating sexual dimorphism that male mice are more adversely affected by this condition. Consistent with the observations, the effects of LPS on muscle catabolism were also less pronounced in the female tumor mice compared to the male tumor mice.

4. Tumor-derived COX-2/PGE2 and host gut-originated LPS synergistically amplify hypothalamic inflammation

Our *in vitro* studies showed that tumor-derived COX-2/PGE2 played a key role in amplifying hypothalamic inflammation. In this animal study, we conducted a series of analyses to further explore the relationship among COX-2 enzyme expression in tumor tissue, plasma PGE2 levels, hypothalamic inflammation, and cancer-related behaviors such as food intake and skeletal muscle mass. The expression of COX-2 enzyme in tumor tissue was confirmed by immunofluorescence staining (Fig. 4k-o). As indicated by various cell type markers, we found that COX-2 (shown in red) was predominantly expressed in tumor cells (marker PanCK shown in white) instead of in immune cells (marker CD45 shown in yellow). Plasma PGE2 concentrations were significantly higher in the tumor-bearing mice compared to the sham mice, and LPS exposure did not affect plasma PGE2 levels (Fig. 4a,d). Furthermore, plasma PGE2 concentrations were higher in the female tumor mice compared to the male tumor mice. Correlation analysis revealed a significant negative correlation between plasma PGE2 concentrations and both food intake (Fig. 4h) and gastrocnemius mass (Fig. 4i) across all tumor mice. This indicates that higher plasma PGE2 levels are associated with cancer progression and perhaps cachexia development, possessing prognostic value for cancer.

To investigate the influence of the tumor on the host intestine, we examined intestinal permeability and LPS translocation. To this end, we measured, in female mice only, the uptake of 4000-Da FITC-Dextran in all mouse blood 4 h after gastric gavage. Plasma FITC levels showed no differences between the tumor mice receiving saline injection, the sham mice receiving LPS injection, and the sham mice receiving saline injection (Fig. 4g). In contrast, LPS exposure increased plasma FITC levels up to several-fold in tumor mice (8377 ng/mL vs 1310 ng/mL, $P < 0.0001$ in the sham + LPS group, and 1620 ng/mL, $P < 0.0001$ in the tumor + saline group). Next, plasma LPS concentrations were measured to determine the contribution of its translocation resulted from impaired GI barrier function. Plasma LPS concentrations were higher in the tumor mice receiving LPS, compared to the tumor mice receiving saline ($P < 0.0001$) or the sham mice receiving LPS ($P < 0.0001$) in both sexes (Fig. 4b,e). In both sexes, plasma LPS levels in the tumor mice receiving saline were slightly higher compared to the sham mice receiving LPS, but this change was not significant. In line with the effects on plasma LPS levels, a prominent rise in plasma IL-6 levels was observed in the tumor mice receiving LPS ($P < 0.0001$) (Fig. 4c,f). Additionally, with LPS treatment, both tumor mice and sham mice exhibited altered expression of intestinal integrity/permeability marker genes in colon tissue (Supplementary Fig. 4a). Compared to sham mice, tumor mice displayed an decreased cecum mass, with corresponding histological changes observed in the colon and cecum tissues, indicating compromised intestinal integrity (Supplementary Fig. 4b,c,d).

Contour plots were produced to visualize the combined influence of PGE2 and LPS on markers of hypothalamic inflammation (Fig. 4j). In male mice, hypothalamic *Cxcl2* and *Ccl2* expression plotted against plasma PGE2 and LPS showed patterns consistent with hypothalamic inflammation increasing at higher levels of both tumor-derived PGE2 and gut-originated LPS. In female mice, hypothalamic *Cxcl2* and *Ccl2* expression plots showed a pattern that was relatively more determined by plasma levels of LPS than of PGE2.

5. Validation of tumor-specific COX-2 knockout.

To explore the role of COX-2 in pancreatic cancer, we proceeded with CRISPR/Cas9–mediated knockout (KO) of *Ptgs2* (coding gene for COX-2) in the mouse pancreatic cancer KPC cell line (Fig. 5a). This cell line is derived from the same parental line as 4662 but induces a more aggressive cancer phenotype when implanted orthotopically into mice (Olson et al., 2021). The *Ptgs2*-KO resulted in a notable reduction in COX-2 protein expression (Fig. 5b) and a significantly reduced *Ptgs2* gene expression (Fig. 5c) within cells, as well as a corresponding reduction of PGE2 in the medium (Fig. 5d).

It is of relevance to note that COX-2 knockout in tumors has been reported to suppress tumor growth in mice (Markosyan et al., 2019). To assess tumor growth, we monitored tumor volume in mice via ultrasound scan after tumor implantation (Supplementary Fig. 5f), and also observed daily for their sickness behavior (Fig. 5a). We subsequently confirmed a marked reduction in *Ptgs2* gene expression within tumor tissues ($P < 0.001$) (Fig. 5f). The plasma PGE2 level was significantly lower than that of the *Ptgs2*-WT group ($P < 0.001$) (Fig. 5g). These analyses indicate a significant reduction in COX-2 expression in mice bearing *Ptgs2*-KO tumors.

6. Tumor-specific COX-2 knockout attenuates hypothalamic inflammation and improves survival.

Due to the slower growth features of *Ptgs2*-KO tumors, mice bearing *Ptgs2*-KO tumors showed no difference in behaviors compared to the sham mice within a short observation period. At the same time, both *Ptgs2*-KO tumor mice and *Ptgs2*-WT tumor mice developed tumors (Fig. 5e). Furthermore, *Ptgs2*-WT tumor mice developed apparent features of cachexia, including significantly lower daily food intake (Fig. 6a) and cumulative food consumption (Supplementary Fig. 5a), increased daily food orts (Supplementary Fig. 5c), as well as decreased skeletal muscle mass and cecum mass compared to the sham mice (Fig. 6b, Supplementary Fig. 5e). Two *Ptgs2*-WT tumor mice developed severe hemorrhagic ascites. However, these cachectic phenotypes were not observed in *Ptgs2*-KO tumor mice (Fig. 6a,b; Supplementary Fig. 5a-e).

We demonstrated that LPS could increase hypothalamic inflammation and intestinal permeability (Fig. 3, Fig. 4). To facilitate a more explicit comparison between *Ptgs2*-KO tumor mice and *Ptgs2*-WT tumor mice, we administered LPS to both groups to enlarge the signaling distinction and to better observe signaling events during an inflammatory challenge.

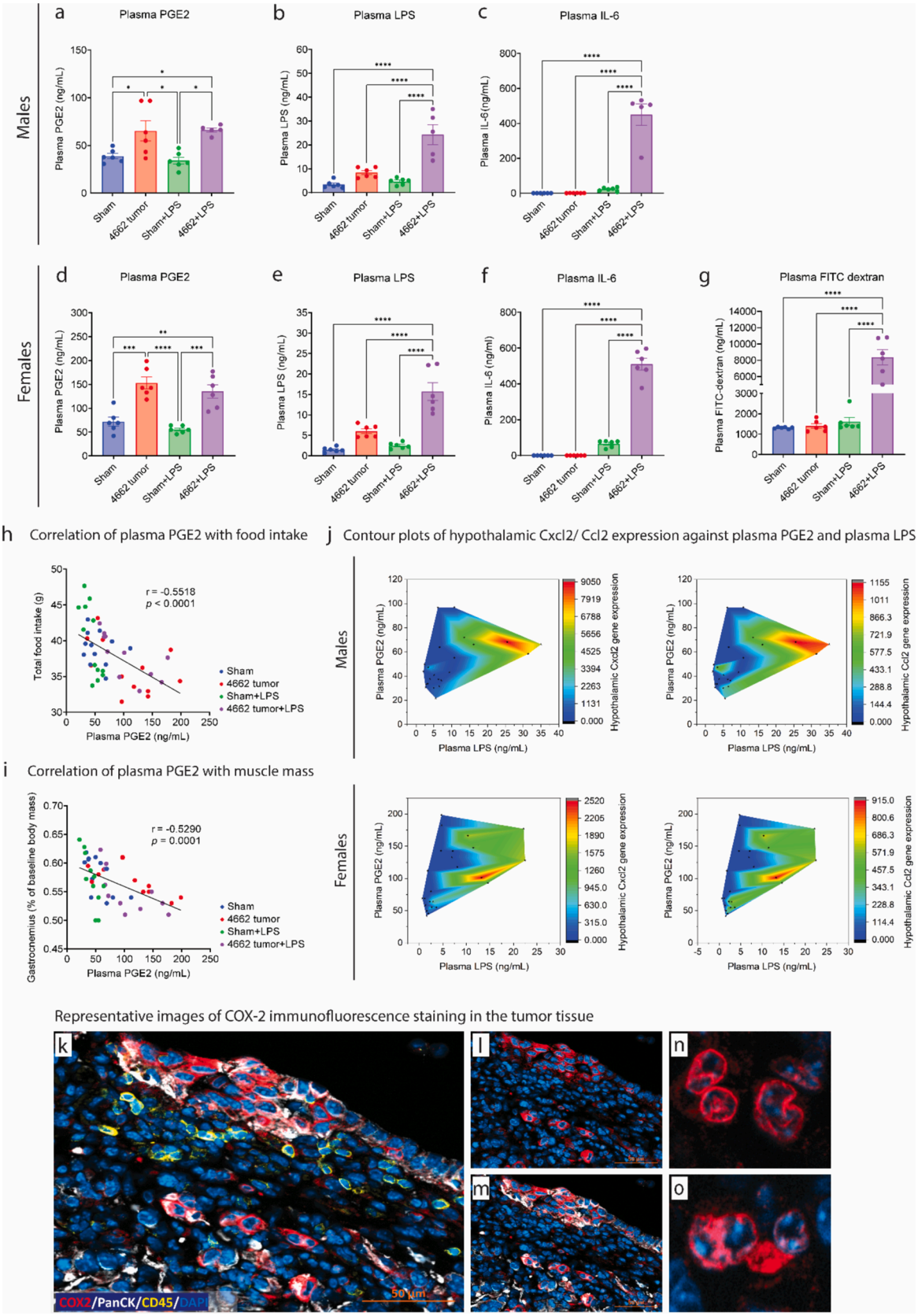

(caption on next page)

Fig. 4. Tumor-derived COX-2/PGE2 and host gut-originated LPS synergistically amplify hypothalamic inflammation. Plasma PGE2 concentration in **a** male and **d** female cohorts. Plasma LPS concentration in **b** male and **e** female cohorts 4 h after LPS IP injection at a dose of 1.5 ug/g body weight, plasma IL-6 concentration in **c** male and **f** female cohorts, and **g** plasma fluorescein isothiocyanate (FITC-)Dextran concentration (a marker for intestinal permeability) in female cohorts. Plasma FITC dextran concentrations (λex = 485; λem = 535 nm) were measured 4 h after FITC dextran gavage at a dose of 0.6 mg/g body weight. Linear regression analysis between plasma PGE2 concentration and **h** total food intake or **i** gastrocnemius mass. **j** Contour plots of hypothalamic *Cxcl2* and *Ccl2* expression (Relative Quantity) plotted against plasma PGE2 (ng/mL) and LPS (ng/mL) concentrations in male and female cohorts, X variable = plasma LPS (ng/mL); Y variable = plasma PGE2 (ng/mL); Z variable = hypothalamic *Cxcl2/ Ccl2* expression (Relative Quantity from low to high shown as blue to red). Representative images of COX-2 immunofluorescence staining in the tumor tissue: **k** The expression of COX-2 enzyme (shown in red), tumor cell marker Pancytokeratin (PanCK, shown in white), immune cell marker CD45 (shown in yellow), and nuclear counterstain DAPI (shown in blue); **l** The expression of COX-2 enzyme (shown in red) and nuclear counterstain DAPI (shown in blue); **m** The expression of COX-2 enzyme (shown in red), tumor cell marker Pancytokeratin (PanCK, shown in white), and nuclear counterstain DAPI (shown in blue); **n**, **o** Representative images at cellular level of the location of COX-2 enzyme expression. Magnifications, ×10 (scale bar = 50 μm). N = 6 per group except for male 4662 + LPS (N = 5). All data were expressed as mean ± SEM. Data represented in **a-g** were analyzed by one-way ANOVA with Bonferroni's post hoc test. Data represented in **h**, **i** were analyzed by simple linear regression and two-tailed correlation analyses. *$p \leq 0.05$, **$p \leq 0.01$, and ***$p \leq 0.001$, ****$p \leq 0.0001$. (For interpretation of the references to colour in this figure legend, the reader is referred to the web version of this article.)

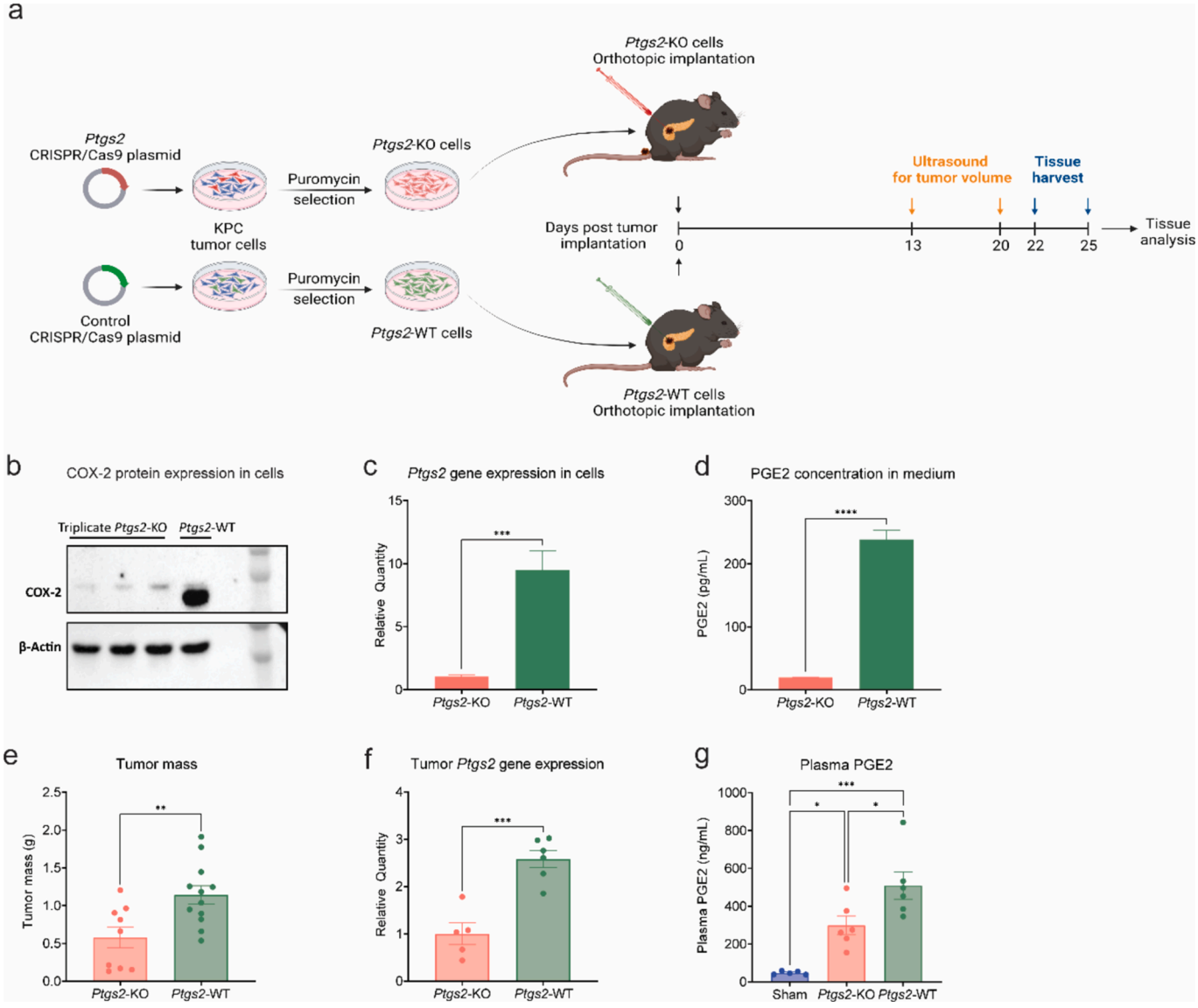

Fig. 5. Validation of tumor-specific COX-2 knockout. **a** Experimental design. The left panel: CRISPR/Cas9-mediated *Ptgs2* knockout (*Ptgs2*-KO) and *Ptgs2* wild type (*Ptgs2*-WT) in KPC pancreatic tumor cells. The right panel: *in vivo* tumor study with the two types of KPC tumor cells (*Ptgs2*-KO vs *Ptgs2*-WT). **b** COX-2 protein expression, **c** relative *Ptgs2* gene expression, and **d** PGE2 levels in both *Ptgs2*-KO and *Ptgs2*-WT KPC tumor cells. **e** Terminal tumor mass, **f** relative *Ptgs2* gene expression in tumor tissues, and **g** plasma PGE2 levels in both *Ptgs2*-KO and *Ptgs2*-WT KPC tumor mice along with sham-operated control mice at the predetermined study endpoint (day 22–25 post-orthotopic tumor cell implantation, depending on the severity of the tumor mouse illness). Sham = blue (N = 5), *Ptgs2*-KO = red (N = 5), *Ptgs2*-WT = green (N = 6). All data were expressed as mean ± SEM. Data represented in **c-f** were analyzed by two-tailed Student's *t* test. **g** Analyzed by one-way ANOVA with Bonferroni's post hoc test. *$p \leq 0.05$, **$p \leq 0.01$, and ***$p \leq 0.001$, ****$p \leq 0.0001$. (For interpretation of the references to colour in this figure legend, the reader is referred to the web version of this article.)

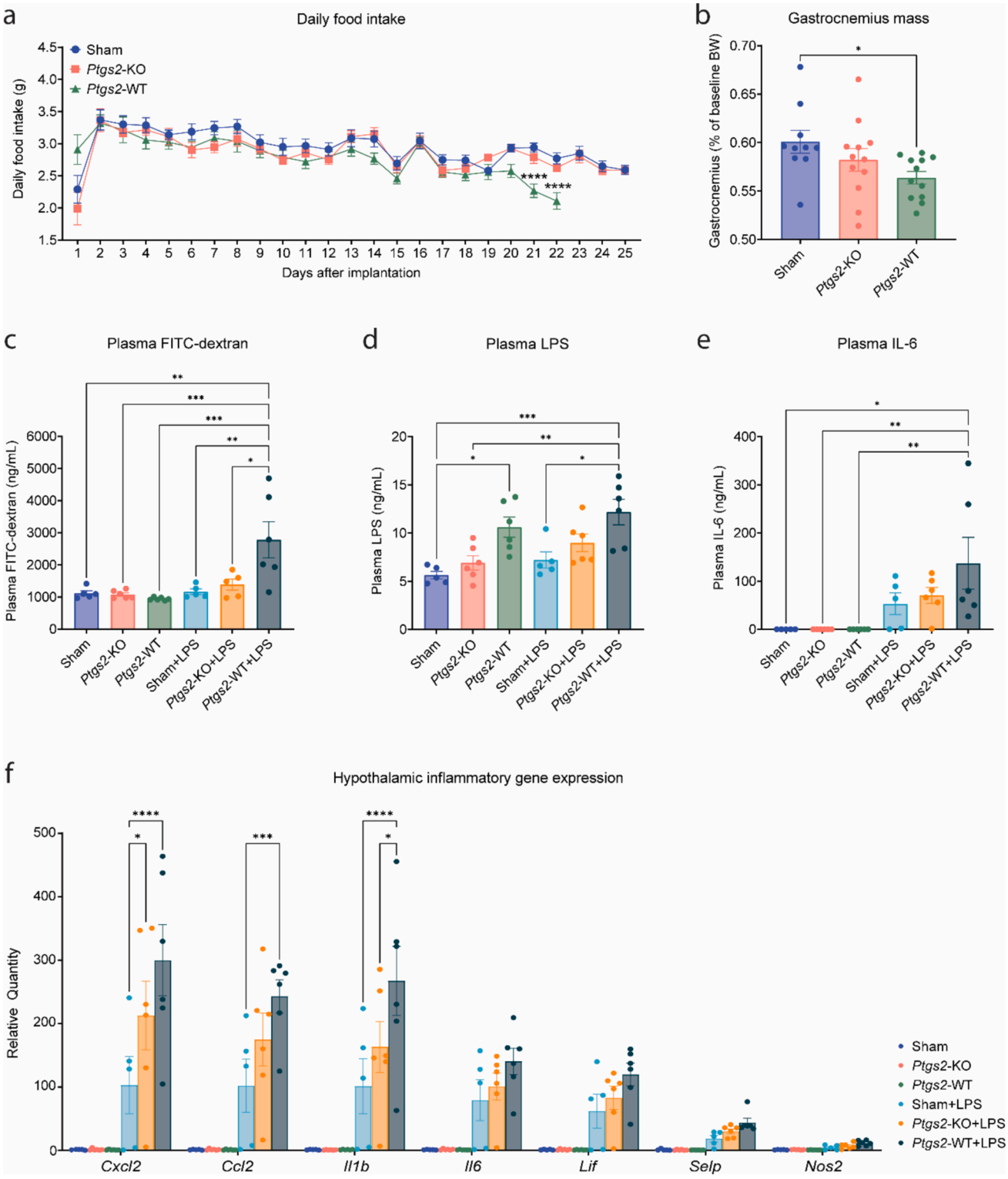

Fig. 6. Tumor-specific COX-2 knockout attenuates hypothalamic inflammation in KPC pancreatic tumor mice. **a** Daily food intake. **b** Terminal gastrocnemius mass normalized to baseline body mass. **c** Terminal intestinal permeability (barrier dysfunction) as measured using FITC-dextran. The plasma FITC dextran concentrations (λex = 485; λem = 535 nm) were measured 4 h after FITC dextran gavage at a dose of 0.6 mg/g body weight. **d** Terminal plasma LPS concentrations measured 4 h after LPS IP injection at a dose of 1.5 ug/g body weight. **e** Terminal plasma IL-6 concentration. **f** RT-PCR analysis in the hypothalamus tissues for pro-inflammatory transcripts (represented as relative quantity to sham controls). Sham: N = 5, *Ptgs2*-KO: N = 6, *Ptgs2*-WT: N = 6, Sham + LPS: N = 5, *Ptgs2*-KO + LPS: N = 6, *Ptgs2*-WT + LPS: N = 6. All data were expressed as mean ± SEM. Data represented in **a, f** were analyzed by two-way ANOVA with Bonferroni's post hoc test. **b-e** Analyzed by one-way ANOVA with Bonferroni's post hoc test. *$p \leq 0.05$, **$p \leq 0.01$, and ***$p \leq 0.001$, ****$p \leq 0.0001$.

Plasma FITC levels were not different between *Ptgs2*-KO tumor mice and sham mice after LPS challenge. In contrast, plasma FITC levels showed a significant increase in *Ptgs2*-WT tumor mice after LPS challenge (Fig. 6c). This coincided with an increase in plasma LPS concentrations in *Ptgs2*-WT tumor mice with or without LPS challenge (Fig. 6d), in line with increased intestinal permeability. Interestingly, *Ptgs2*-KO tumor mice with or without LPS challenge exhibited slightly higher plasma LPS levels compared to the sham mice, and the changes were not significant (Fig. 6d). Subsequently, plasma IL-6 levels increased in *Ptgs2*-WT tumor mice after LPS challenge (Fig. 6e). These results indicate that exogenous LPS challenge induced a more pronounced overall inflammatory response in *Ptgs2*-WT tumor mice compared to *Ptgs2*-KO tumor mice, and that *Ptgs2*-WT tumor mice displayed a higher susceptibility to endotoxin and a greater variation in intestinal permeability than *Ptgs2*-KO tumor mice.

As anticipated, LPS induced a lower degree of hypothalamic inflammation in *Ptgs2*-KO tumor mice compared to *Ptgs2*-WT tumor mice (Fig. 6f). The *Ptgs2*-KO tumor mice showed a mild, albeit statistically insignificant increase in the expression of most inflammatory genes, with the exception of *Cxcl2* expression ($P < 0.05$), compared to the sham mice. In contrast, the *Ptgs2*-WT tumor mice displayed a considerable elevation in hypothalamic inflammation upon LPS challenge. Specifically, the *Ptgs2*-WT tumor mice with LPS challenge exhibited significant increases in the expression of *Cxcl2* ($P < 0.0001$), *Ccl2* ($P < 0.001$), and *Il1b* ($P < 0.0001$) when compared to the sham mice with LPS challenge. Notably, the expression of *Il1b* in *Ptgs2*-WT tumor mice with LPS challenge was significantly higher than that of *Ptgs2*-KO tumor mice with LPS challenge ($P < 0.05$). This indicates that tumor-specific COX-2 knockout effectively attenuates LPS-induced hypothalamic inflammation.

It is noteworthy that two sham mice and one *Ptgs2*-KO mouse did not exhibit a response to the LPS stimulation (Fig. 6e,f). Such variations in responsiveness are not uncommon and are likely linked to differences in immune system reactivity. The literature (Cook et al., 2013; Peppler et al., 2016) suggests that this phenomenon may be attributed to voluntary wheel-running training, which was indeed provided to the mice in our studies for a duration of 21 days preceding the orthotopic tumor implantation.

To assess the impact of tumor-specific COX-2 knockout on tumor growth and tumor-related mortality, we conducted survival experiments. The survival time of *Ptgs2*-KO tumor mice was significantly longer compared to *Ptgs2*-WT tumor mice, with a median survival time of 45.5 vs 28 days (*Ptgs2*-KO vs *Ptgs2*-WT, $P < 0.0001$) (Fig. 7a), although initial body weights and terminal tumor mass were no difference between two groups (Fig. 7b,c). Collectively, these findings suggest that the specific knockout of COX-2 within the tumor cells slowed tumor growth, mitigated LPS-induced hypothalamic inflammation, and attenuated cachexia, ultimately leading to markedly improved survival outcomes.

3. Discussion

Our findings offer novel insights into the intricate interplay between the hypothalamus, tumors, and the intestine, particularly regarding intestinal barrier function, adding to our understanding of cancer, and cancer-associated anorexia-cachexia. Our most remarkable discovery herein pertains to the key role of tumor-associated COX-2 in fuelling hypothalamic inflammation. Our study sheds light on the intricate interactions involving PGE2, a major product of COX-2 in tumors, which directly provokes hypothalamic inflammation through the EP4 receptor, and indirectly amplifies hypothalamic inflammation via NF-κB pathways in the presence of host gut-derived PAMPs. Furthermore, the knockout of COX-2 within the tumor result in decreased hypothalamic inflammation, retarded tumor growth, and improved survival.

Underlying mechanisms behind hypothalamic inflammation were explored with a mouse hypothalamic neuronal cell line model (Li et al., 2022). This cell line is originally derived from a male mouse which might be of relevance considering the sex differences found in the present study. We demonstrate that PGE2 is abundantly present in tumor secretomes and able to amplify LPS-induced hypothalamic inflammation. Results from our current research, in conjunction with previous studies (Li et al., 2022), suggest that the effects of tumor-derived PGE2 on the hypothalamus likely arise from both direct and indirect mechanisms. While the direct effects of PGE2 are mediated by EP receptors, PGE2 also appears to contribute to an increased influx of PAMPs from the intestine, which in turn further contributes to hypothalamic inflammation.

Using a series of antagonists and agonists for the EP receptors we collect evidence that the EP4 receptor plays a major role in the direct effects of PGE2 on LPS-induced hypothalamic inflammation. The involvement of EP receptors in hypothalamic neurons is a novel discovery. Previous studies on EP receptors primarily focused on tumorigenesis. Specifically, EP2 null mice showed reduced tumor multiplicity and lung tumor burden (Keith et al., 2006). Mice homozygously deficient in EP1 and EP4 receptors were partially resistant to colon cancer (Hawcroft et al., 2006; Kawamori et al., 2005). At the same time, activation of the EP3 receptor has been linked to angiogenesis and tumor growth in lung cancer (Amano et al., 2003). We also find that the expression of EP1 and EP4 receptors is much higher than that of EP2 and EP3 receptors in the hypothalamic neuronal cells, further underlining the relevance of the EP4 receptor in hypothalamic neuronal inflammation. To our knowledge, this study provides the first evidence that tumor-derived PGE2 binds to EP4 receptors in hypothalamic neuronal cells, thereby amplifying LPS-induced hypothalamic inflammation. The precise locations of the PGE2 receptors mediating the CNS response to PGE2 remain unknown. By re-analyzing single-cell RNA sequencing data

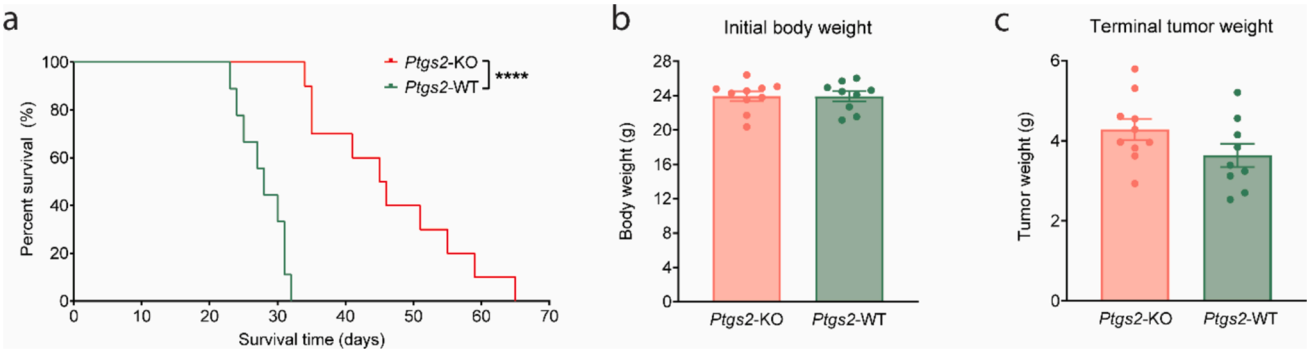

Fig. 7. Tumor-specific COX-2 knockout improves survival. **a** Survival rate, **b** initial body weight pre-tumor implantation, and **c** terminal tumor weight in both *Ptgs2*-KO and *Ptgs2*-WT KPC pancreatic tumor mice. *Ptgs2*-KO: N = 10, *Ptgs2*-WT: N = 9. All data were expressed as mean ± SEM. Data represented in **a** were analyzed by Log-rank (Mantel-Cox) test. **b, c** were analyzed by two-tailed Student's *t* test. $^{*}p \leq 0.05$, $^{**}p \leq 0.01$, and $^{***}p \leq 0.001$, $^{****}p \leq 0.0001$.

(Campbell et al., 2017), we find that PGE2 receptors, especially the EP4 receptors are mainly expressed in hypothalamic neurons of the arcuate nucleus of adult mice. Of relevance is that neurons are among the first cell populations in the hypothalamus that encounter stimuli from the blood (Campbell et al., 2017). Based on these collective findings, we hypothesize that in the hypothalamus, EP4 receptors present in neurons are the first to sense PGE2 secreted by tumor cells.

Both LPS and Pam are PAMPs that can bind to TLR4 and TLR1/2 on hypothalamic cells. This process induces the expression of proinflammatory molecules, inducing inflammation and eventually neuronal death in the hypothalamic arcuate nucleus, a center of feeding regulation (Shabab et al., 2017). Downstream signaling of TLRs involves NF-κB and CREB (Swanson et al., 2020). In the present study, the inhibition of NF-κB reduced inflammation significantly. We hypothesize that NF-κB is likely to be the main regulatory target of PGE2 in amplifying hypothalamic IL-6 secretion. Simultaneous inhibition of both EP4 and TLR/NF-κB eliminated IL-6 secretion. Other studies demonstrated that inhibiting hypothalamic IKKβ/NF-κB could restore energy imbalance in obesity (Zhang et al., 2008). Furthermore, prevention of the activation of hypothalamic or cerebral IKK-β and NF-κB resulted in aging retardation and lifespan extension in mice (Zhang et al., 2013). Evidence for the role of EP4 acting as a functional receptor for PGE2 in controlling systemic inflammation through the activation of neuronal circuits involved in the glucocorticoid axis is further supported by another study (Zhang and Rivest, 2000). While targeted inhibition of hypothalamic inflammation, for instance, through the co-suppression of PGE2 receptors and the TLR signaling pathway, is receiving scientific interest, there are to our knowledge no clinical developments.

It is well-known from previous studies, including those in patients, that COX-2 expression is often elevated in tumors. This enhanced COX-2 expression leads to an increased release of prostaglandins and contributes to the elevated inflammatory state that is frequently associated with cancer (Bell and Zelenay, 2022; Wang and Dubois, 2006). Among the prostaglandins, PGE2 is predominantly produced in many human solid tumors, including colon (Karpisheh et al., 2019; Rigas et al., 1993), lung ("PGE2 Produced by Lung Cancer Suppresses Immune Function Through T-regulatory Cells and can be Blocked by the COX2 Inhibitor Celebrex," 2005), and pancreatic (Charo et al., 2013; Hasan et al., 2008) cancers. While clinical evidence directly linking COX-2 expression in tumors in patients with cancer-cachexia is not yet available, our results align with observations indicating that COX inhibition through NSAIDs can improve survival outcomes in cachectic cancer patients. COX-2 is known to be predominantly present in immune cells such as macrophages (van Dierendonck et al., 2022). However, here we demonstrate that COX-2 is concentrated in cancer cells more than immune cells. Similar results were reported by other studies, demonstrating that COX-2 was present in large amounts in tumor cells (Bell et al., 2022; Bell and Zelenay, 2022; Zheng et al., 2019).

Systemic inflammation is a hallmark of cancer in patients (Argilés et al., 2019). As shown in several studies, including those conducted by our group, systemic inflammation can trigger an elevated inflammatory response within various tissues, including the gastrointestinal tract, leading to functional changes. In our study, it is evident that there are significant impairments in intestinal barrier function in tumor-bearing mice; however, it is primarily the combination of a tumor and LPS that has the most adverse effects on intestinal barrier function. Other studies demonstrated that PGE2 could impair colonic epithelial barrier integrity (Lejeune et al., 2010; Zhou et al., 2020). Our findings further underline previous reports that an impaired intestinal barrier function can exacerbate the inflammatory process by increasing the uptake of LPS and other PAMPs. Such an elevation of plasma LPS levels has also been reported in patients with colorectal cancer and colonic hyperpermeability (de Waal et al., 2020).

Hypothalamic inflammation has a key contribution to cancer progression and cachexia development as the hypothalamus regulates energy metabolism, appetite, and fatigue (Dwarkasing et al., 2016b; Van Norren et al., 2017), thus significantly impacting mortality (Burfeind et al., 2016b). Hypothalamic inflammation and increased intestinal permeability can be also induced by chemotherapy and radiation. Clinical cases of PICC (Peripherally inserted central catheter) line use in chemotherapy frequently coincided with increased blood LPS levels (Valdés-Ferrada et al., 2020). Our data consistently show elevated hypothalamic inflammation by LPS in the mouse model of pancreatic cancer. Similar observations were made in a rat mammary carcinoma model, where tumors exacerbated pro-inflammatory gene expression in the central nervous system in response to LPS and the induction of neuroinflammatory pathways (Pyter et al., 2014). Previous *in vitro* studies also showed that various tumor secretomes, including those from colon, lung, and pancreatic cancer, could enhance LPS-induced hypothalamic inflammation (Li et al., 2022). Remarkably, our study reveals sexual dimorphism in LPS-induced hypothalamic inflammation associated with cancer. Female mice displayed an apparently higher tolerance to LPS stimulation, as evidenced by a lower degree of hypothalamic inflammation and less muscle loss compared to male mice. This contrasts with reports of higher peripheral and central inflammation in females compared to males following LPS stimulation (Dockman et al., 2022) but aligns with findings from mouse depression models (Millett et al., 2019). Our data consistently demonstrate higher plasma LPS levels in males compared to females.

A potentially imminent therapeutic strategy, based on the current results combined with previous findings, could be the targeted modulation of COX-2 activity. Our previous *in vitro* study demonstrated that the COX-2 inhibitor celecoxib reduced PGE2 formation in tumor cells (Li et al., 2022). Here we show that a tumor-specific *Ptgs2* gene knockout model attenuates hypothalamic inflammation during pancreatic cancer, with a slower tumor growth rate and more prolonged survival. A recent study corroborated the assertion that PDAC-derived PGE2 facilitated tumor proliferation. The results of that study indicate that targeting tumor-derived COX-2 induces reprogramming of the tumor microenvironment and effectively regulates the disease state (Caronni et al., 2023). Other studies have suggested that micro RNAs (miRs) directly modulating *Ptgs2* expression are of potential interest in different cancers (Ercolano et al., 2019). Furthermore, *Ptgs2* knockout inhibited melanoma (Ercolano et al., 2019) and pancreatic cancer tumorigenesis (Markosyan et al., 2019).

The aforementioned findings raise the question: Is COX-2 inhibition with COX-2 inhibitors already on the market clinically the way to go in cancer research? Essential factors to be considered in this regard include: 1) Currently used COX-2 inhibitors and traditional NSAIDs are associated with adverse cardiovascular side effects (Schjerning et al., 2020) and reported to increase intestinal permeability (Burian and Geisslinger, 2003). This represents a significant concern, particularly in light of the role of intestinal permeability described in this paper. 2) Non-targeted COX inhibition subsequently reduces multi-metabolites of arachidonic acid. The enzyme COX-2 generates diverse metabolites in addition to PGE2. These include prostaglandins like PGE3, PGI2, PGD2, and PGF2α, but also, for example, thromboxanes (Wang and Dubois, 2006). Additionally, the enzyme COX-1 generates PGE1 among other substances, which is partially inhibited by common COX-2 inhibitors, as overly specific inhibition of COX-2 can cause serious cardiovascular side effects (Schjerning et al., 2020). Inhibition of COX will thus lead to reduced PGE2 and many other COX metabolite production. Prostaglandin I2, among the metabolites, shows a protective effect against injury, cell adhesion, and vessel contraction, and inhibits intestinal epithelial permeability and apoptosis (Pochard et al., 2021). The functions of PGE2 are a double-edged sword. It is reported to increase tumoral progression in the microenvironment and regulate tumor immune evasion (Finetti et al., 2020). However, PGE2 improves myogenic differentiation in primary myoblasts (Mo et al., 2015; Shimonty et al., 2023), and regulates the proliferation of endothelial cells in the gastrointestinal tract, mediating normal platelet function and renal blood flow (De et al., 2021). Considering these factors, therapeutic

inhibition of COX-2 will require a tumor-specific rather than a systemic approach. A search in the Google Patents database ("Google Patents," n. d.) revealed that such an approach is indeed receiving considerable attention.

Taken together, elevated hypothalamic inflammation is shown to be associated with tumor-derived COX-2 during cancer, as well as increased intestinal permeability. We hypothesize that gut-originated PAMPs reach the hypothalamus and activate the TLR/MyD88/NF-κB pathway. At the same time, tumor-derived COX-2 accelerates the secretion of PGE2, thereby activating the EP4 receptor and its downstream pathway in the hypothalamus, synergistically activating the NF-κB pathway, and amplifying hypothalamic inflammation. Our findings can be summarized and explained by the model as proposed in Fig. 8.

A limitation is the absence of labeling for the exogenous LPS used in this study, as tumor-bearing mice exhibit more resistance to endogenous LPS than exogenous LPS. Future investigations could monitor the origins of LPS and compare the different responses of hosts to exogenous LPS triggered by chemotherapy, etc., with those to endogenous LPS present in the persistent tumor environment.

Based on the data presented here, we propose COX-2 and EP4 as potential therapeutic targets for attenuating hypothalamic inflammation in cancer. Future studies could be initiated to develop hypothalamus-specific EP4 knockout strategies, given the current challenges in guaranteeing the viability of *in vivo* EP4 knockout mice. Furthermore, the modulation of COX-2 expression within the tumor or genetic engineering of EP4 in the hypothalamus necessitates effective delivery systems for targeted transport, such as nanocarriers (Zhao et al., 2020). The discovery of efficient inhibitors and delivery systems holds transformative potential in enhancing the success rates of selective drug development for the treatment of cancer.

4. Materials and methods

4.1. In vitro studies

Reagents

REAGENT	SOURCE
HiPerSolv CHROMANORM® (≥99.9 %)	VWR Chemicals
BMS-345541	Sigma-Aldrich
Butylated hydroxytoluene	Sigma-Aldrich
Ethanol	Sigma-Aldrich
Formic acid (99 %)	Biosolve Chemicals
GW9662	R&D systems
KG-501 (Naphthol AS-E phosphate)	MedChemExpress
L-161982 (EP4 antagonist)	Tocris
L-798,106 (EP3 antagonist)	Tocris
Lipopolysaccharide (O111:B4; LPS)	Sigma-Aldrich
Methanol	VWR Chemicals
MMG 11 (TLR2 antagonist)	Tocris
Pam3CysSerLys4 (Pam3Cys-SKKKK)	EMC Microcollections
PF-04418948 (EP2 antagonist)	Tocris
Prostaglandin D2	R&D systems
Prostaglandin E1	Cayman Chemicals
Prostaglandin E2	R&D systems
Prostaglandin E3	R&D systems
Prostaglandin F2α	Sanbio B.V.
Rosiglitazone	Tocris
SC-51089 (EP1 antagonist)	Tocris
ST 2825 (MyD88 inhibitor)	MedChemExpress
Sulprostone (EP1/ EP3 agonist)	Abcam
TAK 242 (TLR4 inhibitor)	Tocris
TCS 2510 (EP4 agonist)	Tocris
Cox-2 CRISPR/Cas9 KO Plasmid (m)	Santa Cruz
Control CRISPR/Cas9 Plasmid	Santa Cruz
Cox-2 HDR Plasmid (m)	Santa Cruz
UltraCruz® Transfection Reagent	Santa Cruz
Puromycin dihydrochloride, 25 mg	Santa Cruz
COX-2 (D5H5) XP® Rabbit mAb #12282	Cell Signaling
Trizol	Fisher Scientific
BCA protein assay kit	Thermo Scientific Pierce Products

4.2. Cell culture

The male mouse hypothalamic neuronal cell line (mHypoE-N46, male) was purchased from CELLutions Biosystems (Burlington, Ontario, Canada). The mouse colon carcinoma (C26) cell line and Lewis lung carcinoma (LLC) cell line were purchased from ATCC (Teddington, UK).

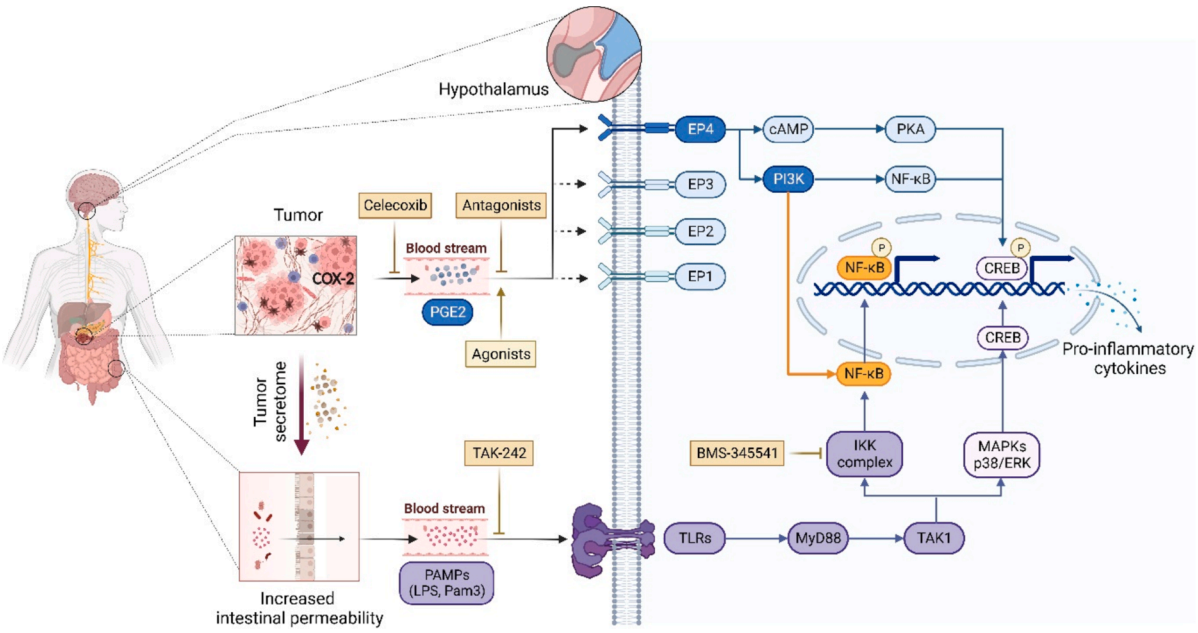

Fig. 8. Hypothetical signaling map of TLRs and PGE2 receptors in amplifying hypothalamic inflammation during cancer. Gut-originated PAMPs reach the hypothalamus and activate the TLR/MyD88/NF-κB pathway. At the same time, tumor-derived COX-2 accelerates the secretion of PGE2, thereby activating the EP4 receptor and its downstream pathway in the hypothalamus, synergistically activating the NF-κB pathway, and amplifying hypothalamic inflammation.

The mHypoE-N46, C26, and LLC cells were grown in Dulbecco's Modified Eagle Medium (DMEM, Corning, USA). All media were supplemented with 10 % fetal calf serum (FCS, Biowest, USA) and 1 % penicillin–streptomycin (Corning, USA), and all cell lines were incubated at 37 °C in a humidified atmosphere with 5 % CO_2.

4.3. CRISPR/Cas9-mediated knockout of Ptgs2 in KPC cell line

Mouse *Ptgs2* CRISPR/Cas9 knockout plasmid (sc-422489), *Ptgs2* HDR plasmid (sc-422489-HDR), Control CRISPR/Cas9 Plasmid (sc-418922), and transfection reagent (sc-395739) were purchased from Santa Cruz Biotechnology (CA, Heidelberg, Germany). 7×10^4 KPC cells were seeded in 3 mL of antibiotic-free standard growth medium per well into a six-well plate 24h prior to transfection. Transfection Reagent was used at a final concentration of 5 % together with a total of 4 μg plasmid (2 μg *Ptgs2* CRISPR/Cas9 KO plasmid with 2 μg *Ptgs2* HDR plasmid) per well. Cells were maintained for 48 h before returning to the growth medium and puromycin selection (20 μg/mL) (sc-108071). The *Ptgs2* HDR plasmid is designed for the repair of the site-specific Cas9-induced DNA cleavage within the *Ptgs2* gene, and contains a puromycin resistance gene to enable selection of stable knockout cells and an RFP gene to visually confirm transfection.

4.4. Western blot

Proteins from cells were lysed in RIPA lysis buffer (89900; Thermo Fisher Scientific) supplemented with phosphatase and protease inhibitors and quantified by BCA Protein Assay kit (Thermo Fisher Scientific). Precast 4 to 15 % polyacrylamide gels were used to separate protein lysates, and proteins were transferred onto nitrocellulose membranes using a Trans-Blot Turbo Semi-Dry Transfer Cell with Trans-Blot Turbo PVDF Transfer Packs (Bio-Rad Laboratories). After blocking with 5 % skim milk, membranes were incubated overnight at 4 °C with primary antibodies against COX-2 (D5H5, 1:1000, #12282, Cell Signaling Technology) and β-Actin (D6A8, 1:4000, #8457, Cell Signaling Technology). Membranes were subsequently incubated with a secondary antibody (Anti-rabbit IgG, HRP-linked Antibody, #7074, Cell Signaling Technology) for 1 h at room temperature. Membranes were developed using Clarity ECL substrate (Bio-Rad Laboratories) and images were acquired with the ChemiDoc MP System (Bio-Rad Laboratories).

4.5. Quantitative RT-PCR

Total RNA was isolated using TRizol Reagent (Thermo Fisher Scientific, 15596018). Complementary DNA (cDNA) was synthesized using the iScript cDNA Synthesis Kit (Bio-Rad Laboratories, Inc., 1708890) following the manufacturer's instructions. Real-Time polymerase chain reaction (RT-PCR) was performed on the CFX 384 Touch Real-Time detection system (Bio-Rad Laboratories, Inc., California, United States), using the SensiMix (BioLine, BIO-83005) protocol for SYBR green reactions. Amplification of Ptgs2 (forward primer 5′-TGAGCAACTATTCCAAACCAGC-3′; reverse primer 5′-GCACGTAGTCTTCGATCACTATC-3′) was normalized with mouse 36B4 expression (forward primer 5′-ATGGGTACAAGCGCGTCCTG-3′; reverse primer 5′-GCCTTGACCTTTTCAGTAAG-3′).

4.6. UPLC-MS/MS analysis of prostaglandins

Concentrations of different prostaglandins in cultured supernatants from tumor cells were determined using a previously published ultra-performance liquid chromatography-tandem mass spectrometry (UPLC-MS/MS) with small adaptations (Balvers et al., 2012).

Standards included Prostaglandin (PG)D_2 (≥98 % purity), PGE_1 (≥98 % purity), PGE_2 (≥98 % purity), PGE_3 (≥98 % purity), 11β-$PGF_2\alpha$ (≥98 % purity), $PGF_2\alpha$ (≥98 % purity), 15-deoxy-Δ12,14-PGJ_2 (≥95 % purity) and were purchased from Cayman Chemicals, supplied by Sanbio (Uden, The Netherlands). In short, prostaglandins were extracted from 200 uL supernatant with 1 mL methanol (MeOH) (≥99.9 %, HiPerSolv CHROMANORM®, ULTRA for LC-MS) containing 1000 pg/mL of PGE_2-d_4 [≥99 % purity deuterated forms (d_1-d_4)]. Samples were shortly vortexed, placed on ice for 30 min and then centrifuged for 5 min at 3000×*g* and 4 °C. Supernatants were combined with 4.8 mL ultrapure water containing 0.125 % formic acid (FA) (99 %, UPLC/MS-CC/SFC) and extracted over HLB solid phase extraction columns (Oasis; 60 mg, 3 cc; Waters Chromatography B.V., Etten-Leur, The Netherlands). The columns were activated by two-times 1 mL MeOH, equilibrated by two-times 1 mL ultrapure water containing 0.1 % FA, loaded with the samples, washed with 2 mL 20 % MeOH in ultrapure water containing 0.1 % FA, and then allowed to dry for 15 min. Compounds were eluted from the column by 2 mL MeOH and collected in borosilicate glass tubes containing 20 μL of 10 % glycerol and 500 μM butylated hydroxytoluene (99 %) in ethanol (EtOH; absolute for analysis). Samples were dried in a TurboVap® evaporator (Biotage, Uppsala, Sweden) at 35 °C under a gentle stream of nitrogen (2.7 L/min). Hereafter, the extracts were reconstituted in 50 μL EtOH. Samples were stored at −80 °C until further analysis. The UPLC-MS/MS system consisted of an Waters I-class fixed-loop UPLC coupled to a Xevo TQ-s triple-quadrupole mass spectrometer. For each run, 10 μL of sample was injected into an Acquity C18 BEH UPLC column (2.1 × 100 mm, 1.7 μm) from Waters Chromatography B.V. (Etten-Leur, The Netherlands). The injected sample was separated on the column using gradient elution with a stable flow of 0.600 mL/min. The gradient started with 95 % A (ultrapure water with 0.1 % FA) and 5 % B (Acetonitrile (ACN; ≥99.9 % purity) with 0.1 % FA). After 0.35 min, the gradient was linearly increased to 70 % A and 30 % B which was achieved at 5.00 min. This was followed by a linear increase to 50 % B, which was achieved at 11.25 min and maintained until 13.25 min. Subsequently, the system was switched to 100 % B, which was achieved at 15.75 min and maintained until 16.75. Hereafter, the column was left to equilibrate at 5 % B for 3.00 min, making a total run time of 19.75 min. During analysis, the column was maintained at 50 °C and the autosampler was cooled to 10 °C. Electrospray ionization in negative mode (ESI-neg) was performed for all analytes. The MS parameters, such as capillary voltage and collision-induced dissociation settings (CID), were tuned by individually infusing all analytes to optimize product ion signal intensity in selective reaction mode (SRM). MS settings were as follows:capillary voltage of 2.7 kV, cone voltage of 30 V, source offset of 30 V, and desolvation temperature of 500 °C. A detailed overview of the applied MS settings is given in Supplementary Table 3. SRM transitions and collision energies (CE) are presented in Supplementary Table 4. Data acquisition and processing was performed using MassLynx version 4.1 (Waters). The limit of detection (LOD) was defined as the concentration corresponding to the smallest integrated peak area included in the calibration curve. Quantification was performed against calibration curve using 1/X^2 weighing QC samples were used to monitor performance of the method.

4.7. Enzyme-linked immunosorbent assays

Levels of IL-6 (R&D Systems, Minneapolis, MN, USA) and PGE2 (Cayman Chemical, Ann Arbor, MI, USA) in cell culture media were detected using mouse ELISA kits according to the manufacturer's instructions. All presented ELISA data were within the range of the respective standard curves. The samples were diluted to fall within the standard curve range when necessary.

4.8. Cell proliferation and toxicity

Effects of different antagonists and agonists on cell proliferation and cytotoxicity were measured using a WST-1 assay kit (Sigma Aldrich, Scheldorf, Germany) and a Lactate Dehydrogenase (LDH) assay kit (Sigma Aldrich, Scheldorf, Germany) according to the manufacturer's

instruction.

5. Experimental animals and design

5.1. Mice

Male and female C57BL/6J WT (JAX catalog number 000664) were purchased from The Jackson Laboratory (Bar Harbor, ME) and maintained in our animal facility. All mice were housed and bred in a dedicated mouse room with a temperature of 26 °C with a 12-h light/dark cycle and 40 % humidity. Animals were provided ad libitum access to food and water (Purina rodent diet 5001; Purina Mills, St. Louis, MO, USA). Animals were aged between 9 and 15 weeks at the time of the study. In behavioral studies, animals were individually housed for acclimation at least 7 days prior to procedures. Except in survival studies, tumor-bearing animals were euthanized according to the endpoints of the tumor study policy. Mouse studies were conducted in accordance with the National Institutes of Health Guide for the Care and Use of Laboratory Animals, and approved by the Institutional Animal Care and Use Committee of Oregon Health & Science University.

5.2. Pancreatic ductal adenocarcinoma cachexia models

Two distinct pancreatic ductal adenocarcinoma (PDAC) cachexia models (4662 and KPC) were used in this study. Both 4662 and KPC are clonogenic cell lines derived from C57BL/6J mice with pancreatic-specific conditional alleles KRASG12D and TP53R172H expression driven by the PDX-1-Cre promoter. The 4662 cell line was generously provided by Robert Vonderheide (4662) (Twyman-Saint Victor et al., 2015), and the KPC cell line was generously provided by Dr. Elizabeth Jaffee (Keenan et al., 2014; Michaelis et al., 2017). Both cell lines were maintained in low glucose Dulbecco's Modified Eagle Medium (Gibco, Thermofisher, Waltham, MA), supplemented with 10 % fetal calf serum (FCS, Biowest, Ann Arbor, MI, USA) and 1 % penicillin–streptomycin (Corning, USA), and maintained at 37 °C in a humidified atmosphere with 5 % CO_2. Under isoflurane anesthesia, a small surgical incision was made in the upper-left quadrant of the abdomen, reflecting the skin layers, fascia, and muscle wall to expose the pancreas. The tail of the pancreas was injected with either 3 million tumor cells suspended in 40 μL of PBS or an equal volume of cell-free PBS. After tumor implantation, the abdominal wall and fascia layers were sutured, followed by two surgical skin clips to close the incision site.

5.3. Ultrasound measurements

Ultrasound scans were performed using a Vevo 2100 system with an MS400 transducer (FUJIFILM Visual Sonics, Toronto, ON, Canada) according to Ito et al (Ito et al., 2021). During ultrasound imaging, mice were anesthetized with 1.5 % isoflurane (EX3 Vaporizer, Patterson Veterinary) and placed dorsally on a warmed scanning platform. Physiological parameters, including cardiac and respiratory cycles, were monitored. Hair was removed with depilatory cream (Nair, Church & Dwight), and warmed ultrasound gel was applied to the ventral chest.

5.4. Analysis of cancer cachexia

Food intake, body mass, and post-procedure health status were monitored daily, and bedding was sifted to collect spilled food (food orts). Mice mortality was observed daily, and the tumor was confirmed by necropsy. When the tumor-bearing mice reached predesignated time points or predetermined criteria for euthanasia, they were given a gavage of 80 mg/mL 4000-Da fluorescein isothiocyanate (FITC-)Dextran (Sigma-Aldrich, St. Louis, MO). The dosage of FITC Dextran for each mouse was calculated by 0.6 mg/g body weight. After 4 h of fasting, mice were injected intraperitoneally with 150 ug/mL LPS (delivered with 0.5 % BSA in saline as a vehicle) or vehicle immediately after receiving the gavage to induce acute inflammation. The dosage of LPS for each mouse was calculated by 1.5 ug/g body weight. After 4 h of food and water restriction, the mice got a dose of a ketamine-xylazine-acepromazine cocktail to induce deep anesthesia. Necropsy tissue analysis included tumor, gastrocnemius, and cecum mass by observers blinded to treatment groups. In addition, the hypothalamus, gastrocnemius, colon, and tumor tissues were immediately flash-frozen for gene expression analysis.

5.5. Intestinal permeability

Intestinal permeability was assessed by determining the transmucosal transport of 4000-Da fluorescein isothiocyanate (FITC-)Dextran (Sigma-Aldrich, St. Louis, MO), according to Johnson et al (Johnson et al., 2015).

5.6. Histology and immunofluorescent staining

At the end of the study, tissues were post-fixed in 4 % PFA overnight at 4 °C and transferred to 70 % ethanol prior to sectioning protocols. After post-fixation, paraffin-embedded histological sections of tumor and colon tissue samples were stained for hematoxylin and eosin (H&E), followed by 10-μM cryostat sectioning.

Free-floating sections were incubated in blocking solution (5 % normal donkey serum in 0.01 M PBS and 0.2 % Triton X-100) for 30 min at room temperature, followed by primary antibody incubation (listed below) overnight at 4 °C. Sections were thoroughly washed with PBS between steps. Sections were mounted on gelatine-coated slides and coverslipped with Prolong Gold anti-fade media with DAPI (Thermofisher).

Fluorescent-based images of tumor tissues were acquired on an ApoTome-Zeiss Microscope. Primary antibodies utilized above are listed respectively: COX-2 (Rabbit, cell signaling, 12282S, 1:500), Pan-CK (Mouse, Invitrogen, MA5-13156, 1:200), and CD45 (Rat, BD Pharmings, 550539, 1:500). The following secondary antibodies were used, all derived from donkey: anti-rabbit A555 (Invitrogen, A31572, 1:400), anti-mouse A647 (Invitrogen, A32787, 1:400), and anti-rat A488 (Invitrogen, A21208, 1:400).

5.7. Enzyme-linked immunosorbent assays

Whole blood was obtained from mice by cardiopuncture, and plasma was isolated using K2EDTA tubes (BD 365974). Mouse plasma was assayed by LPS ELISA (MyBioSource, San Diego, CA), IL-6 ELISA (R&D Systems, Minneapolis, MN, USA), and PGE2 ELISA (Cayman Chemical, Ann Arbor, MI, USA) kits according to manufacturer's instructions.

5.8. Quantitative real-time PCR

Snap-frozen tissues were rapidly homogenized, and RNA was purified with the RNeasy Mini Kit (Qiagen). Samples were then reverse transcribed with the High Capacity cDNA Reverse Transcription Kit (Life Technologies). qRT-PCR was performed using reagents, and TaqMan primer probes listed in Supplementary Table 2. Tissues were normalized to 18S or β-Actin using the ΔΔCt method.

The relative expression was calculated with the ΔΔCt method and normalized to the sham control. Normally distributed ΔCt values were used for the statistical analysis.

5.9. Survival study

Sex, age, and body weight-matched WT mice were implanted with either *Ptgs2*-KO or *Ptgs2*-KO control (*Ptgs2*-WT) tumor cells. All animals were individually housed after implantation and observed daily until death. Tumor appearance was confirmed in all animals, and tumors were dissected and weighed by necropsy.

5.10. Statistics

All statistical analyses were performed in GraphPad Prism 9.5.1 software and Origin 9.0 software. Quantitative data are reported as mean ± standard error. Two-tailed Students *t* tests were performed when comparing two groups. When comparing more than two groups of a single genotype, One-way ANOVA was utilized. Correlation analyses were performed after assessment of normality using Shapiro–Wilk tests, demonstrating that all data analyzed followed a Gaussian distribution (Pearson correlation, parametric data). Two-way ANOVA with Bonferroni multiple comparisons test was utilized when comparing multiple genotypes and treatment groups (sham and tumor). For all analyses, a *P*-value of <0.05 was considered to be statistically significant. For histochemistry analyses, images were representative of at least three separate stainings. Western blot images are representative of at least two separate experiments. All measurements were from distinct samples and not taken from the same sample more than once. When applicable, all statistical tests were performed as two-tailed analyses.

CRediT authorship contribution statement

Xiaolin Li: Writing – review & editing, Writing – original draft, Validation, Software, Methodology, Investigation, Conceptualization. **Xinxia Zhu:** Writing – review & editing, Methodology. **Parham Diba:** Resources. **Xuan Shi:** Investigation. **Frank Vrieling:** Investigation. **Fleur A.C. Jansen:** Investigation. **Michiel G.J. Balvers:** . **Ian de Bus:** . **Peter R. Levasseur:** Resources. **Ariana Sattler:** Investigation. **Paige C. Arneson-Wissink:** Investigation. **Mieke Poland:** Resources. **Renger F. Witkamp:** Writing – review & editing, Supervision, Project administration, Funding acquisition. **Klaske van Norren:** . **Daniel L. Marks:** Writing – review & editing, Supervision, Resources, Project administration, Funding acquisition.

Declaration of competing interest

The authors declare the following financial interests/personal relationships which may be considered as potential competing interests: D. L.M. is a consultant, chief medical officer, stockholder, and has received grant funding from Endevica Bio, Inc. D.L.M. is a consultant for Alkermes, Inc. and Pfizer, Inc. X.Z. is a stockholder in Endevica Bio, Inc. The other authors declare no competing interests.

Acknowledgments

We thank Robert Vonderheide (4662) and Drs Elizabeth Jaffee (KPC) for graciously providing the syngeneic pancreatic cancer cell lines used for our studies. We thank Dr Sander Grefte for revising the manuscript. We thank Abby C. Buenafe for helping with the animal study. The graphical abstract and Fig. 6a were made using BioRender (BioRender.com). We acknowledge financial support by the China Scholarship Council to the first author.

Author contributions

X.L., K.V.N., and D.L.M. designed the study. X.L., X.Z., P.D., X.S., F. V., F.A.C.J., P.R.L., A.S., P.C.A.W., M.P., M.G.J.B., and I.D.B. performed experiments. X.L., X.Z., K.V.N., and D.L.M. analyzed the data and contributed with discussion. X.L. wrote the manuscript with input from the other authors. R.F.W., K.V.N., and D.L.M. reviewed and edited the manuscript. All authors approved the final version of the manuscript.

Appendix A. Supplementary data

Supplementary data to this article can be found online at https://doi.org/10.1016/j.bbi.2024.11.002.

Data availability

All data associated with this study are available in the main text, supplementary materials, or source data file. There are no restrictions on data availability. Source data are provided with this paper.

References

Amano, H., Hayashi, I., Endo, H., Kitasato, H., Yamashina, S., Maruyama, T., Kobayashi, M., Satoh, K., Narita, M., Sugimoto, Y., Murata, T., Yoshimura, H., Narumiya, S., Majima, M., 2003. Host prostaglandin E2-EP3 signaling regulates tumor-associated angiogenesis and tumor growth. J. Exp. Med. 197, 221–232. https://doi.org/10.1084/JEM.20021408.

Argilés, J.M., López-Soriano, F.J., Busquets, S., 2019. Mediators of cachexia in cancer patients. Nutrition 66, 11–15. https://doi.org/10.1016/J.NUT.2019.03.012.

Balvers, M.G.J., Verhoeckx, K.C.M., Bijlsma, S., Rubingh, C.M., Meijerink, J., Wortelboer, H.M., Witkamp, R.F., 2012. Fish oil and inflammatory status alter the n-3 to n-6 balance of the endocannabinoid and oxylipin metabolomes in mouse plasma and tissues. Metabolomics 8, 1130–1147. https://doi.org/10.1007/S11306-012-0421-9/TABLES/6.

Bell, C.R., Pelly, V.S., Moeini, A., Chiang, S.C., Flanagan, E., Bromley, C.P., Clark, C., Earnshaw, C.H., Koufaki, M.A., Bonavita, E., Zelenay, S., 2022. Chemotherapy-induced COX-2 upregulation by cancer cells defines their inflammatory properties and limits the efficacy of chemoimmunotherapy combinations. Nat. Commun. 13 (1), 1–17. https://doi.org/10.1038/s41467-022-29606-9.

Bell, C.R., Zelenay, S., 2022. COX-2 upregulation by tumour cells post-chemotherapy fuels the immune evasive dark side of cancer inflammation. Cell Stress 6, 76. https://doi.org/10.15698/CST2022.09.271.

Bindels, L.B., Neyrinck, A.M., Loumaye, A., Catry, E., Walgrave, H., Cherbuy, C., Leclercq, S., Van Hul, M., Plovier, H., Pachikian, B., Bermúdez-Humarán, L.G., Langella, P., Cani, P.D., Thissen, J.-P., Delzenne, N.M., 2018. Increased gut permeability in cancer cachexia: mechanisms and clinical relevance. Oncotarget 9, 18224–18238.

Braun, T.P., Zhu, X., Szumowski, M., Scott, G.D., Grossberg, A.J., Levasseur, P.R., Graham, K., Khan, S., Damaraju, S., Colmers, W.F., Baracos, V.E., Marks, D.L., 2011. Central nervous system inflammation induces muscle atrophy via activation of the hypothalamic–pituitary–adrenal axis. J. Exp. Med. 208, 2449–2463. https://doi.org/10.1084/JEM.20111020.

Braun, T.P., Szumowski, M., Levasseur, P.R., Grossberg, A.J., Zhu, X., Agarwal, A., Marks, D.L., 2014. Muscle atrophy in response to cytotoxic chemotherapy is dependent on intact glucocorticoid signaling in skeletal muscle. PLoS One 9. https://doi.org/10.1371/JOURNAL.PONE.0106489 e106489.

Burfeind, K.G., Michaelis, K.A., Marks, D.L., 2016a. The central role of hypothalamic inflammation in the acute illness response and cachexia. Semin. Cell Dev. Biol. https://doi.org/10.1016/j.semcdb.2015.10.038.

Burfeind, K.G., Michaelis, K.A., Marks, D.L., 2016b. The central role of hypothalamic inflammation in the acute illness response and cachexia. Semin. Cell Dev. Biol. 54, 42–52. https://doi.org/10.1016/J.SEMCDB.2015.10.038.

Burian, M., Geisslinger, G., 2003. Klinische pharmakologie der selektiven COX-2-hemmer. Orthopade 32, 1078–1087. https://doi.org/10.1007/S00132-003-0569-0/TABLES/4.

Campbell, J.N., Macosko, E.Z., Fenselau, H., Pers, T.H., Lyubetskaya, A., Tenen, D., Goldman, M., Verstegen, A.M.J., Resch, J.M., McCarroll, S.A., Rosen, E.D., Lowell, B. B., Tsai, L.T., 2017. A molecular census of arcuate hypothalamus and median eminence cell types. Nat. Neurosci. 20 (3), 484–496. https://doi.org/10.1038/nn.4495.

Caplan, I.F., Maguire-Zeiss, K.A., 2018. Toll-like receptor 2 signaling and current approaches for therapeutic modulation in synucleinopathies. Front. Pharmacol. 9, 417. https://doi.org/10.3389/FPHAR.2018.00417/BIBTEX.

Caronni, N., La Terza, F., Vittoria, F.M., Barbiera, G., Mezzanzanica, L., Cuzzola, V., Barresi, S., Pellegatta, M., Canevazzi, P., Dunsmore, G., Leonardi, C., Montaldo, E., Lusito, E., Dugnani, E., Citro, A., Ng, M.S.F., Schiavo Lena, M., Drago, D., Andolfo, A., Brugiapaglia, S., Scagliotti, A., Mortellaro, A., Corbo, V., Liu, Z., Mondino, A., Dellabona, P., Piemonti, L., Taveggia, C., Doglioni, C., Cappello, P., Novelli, F., Iannacone, M., Ng, L.G., Ginhoux, F., Crippa, S., Falconi, M., Bonini, C., Naldini, L., Genua, M., Ostuni, R., 2023. IL-1β+ macrophages fuel pathogenic inflammation in pancreatic cancer. Nature 623 (7986), 415–422. https://doi.org/10.1038/s41586-023-06685-2.

Charo, C., Holla, V., Arumugam, T., Hwang, R., Yang, P., Dubois, R.N., Menter, D.G., Logsdon, C.D., Ramachandran, V., 2013. Prostaglandin E2 regulates pancreatic stellate cell activity via the EP4 receptor. Pancreas 42, 467–474. https://doi.org/10.1097/MPA.0B013E318264D0F8.

Cook, M.D., Martin, S.A., Williams, C., Whitlock, K., Wallig, M.A., Pence, B.D., Woods, J. A., 2013. Forced treadmill exercise training exacerbates inflammation and causes mortality while voluntary wheel training is protective in a mouse model of colitis. Brain Behav. Immun. 33, 46–56. https://doi.org/10.1016/J.BBI.2013.05.005.

Davis, T.W., Zweifel, B.S., O'Neal, J.M., Heuvelman, D.M., Abegg, A.L., Hendrich, T.O., Masferrer, J.L., 2004. Inhibition of cyclooxygenase-2 by celecoxib reverses tumor-induced wasting. J. Pharmacol. Exp. Ther. 308, 929–934. https://doi.org/10.1124/JPET.103.063099.

De, G.A., Linares, P., Opperman, R.M., Majumder, M., Lala, P.K., Hodivala-Dilke, K., Munoz-Felix, J.M., 2021. Prostaglandin E2 Receptor 4 (EP4) as a therapeutic target to impede breast cancer-associated angiogenesis and lymphangiogenesis. Cancers 13, 942. https://doi.org/10.3390/CANCERS13050942.

de Waal, G.M., de Villiers, W.J.S., Forgan, T., Roberts, T., Pretorius, E., 2020. Colorectal cancer is associated with increased circulating lipopolysaccharide, inflammation and hypercoagulability. Sci. Rep. 10. https://doi.org/10.1038/S41598-020-65324-2.

Dockman, R.L., Carpenter, J.M., Diaz, A.N., Benbow, R.A., Filipov, N.M., 2022. Sex differences in behavior, response to LPS, and glucose homeostasis in middle-aged mice. Behav. Brain Res. 418, 166–4328. https://doi.org/10.1016/j.bbr.2021.113628.

Dwarkasing, J.T., Witkamp, R.F., Boekschoten, M.V., Ter Laak, M.C., Heins, M.S., van Norren, K., 2016. Increased hypothalamic serotonin turnover in inflammation-induced anorexia. BMC Neurosci. 17, 1–13. https://doi.org/10.1186/S12868-016-0260-0/TABLES/2.

Ercolano, G., De Cicco, P., Rubino, V., Terrazzano, G., Ruggiero, G., Carriero, R., Kunderfranco, P., Ianaro, A., 2019. Knockdown of PTGS2 by CRISPR/CAS9 system designates a new potential gene target for melanoma treatment. Front. Pharmacol. 10, 488252. https://doi.org/10.3389/FPHAR.2019.01456/BIBTEX.

Finetti, F., Travelli, C., Ercoli, J., Colombo, G., Buoso, E., Trabalzini, L., 2020. Prostaglandin E2 and Cancer: Insight into Tumor Progression and Immunity. Biology 9, 434. https://doi.org/10.3390/BIOLOGY9120434.

Google Patents [WWW Document], n.d. URL https://patents.google.com/ (accessed 10.8.23).

Haroun, E., Kumar, P.A., Saba, L., Kassab, J., Ghimire, K., Dutta, D., Lim, S.H., 2023. Intestinal barrier functions in hematologic and oncologic diseases. J. Transl. Med. 1 (21), 1–19. https://doi.org/10.1186/S12967-023-04091-W.

Hasan, S., Satake, M., Dawson, D.W., Funahashi, H., Angst, E., Go, V.L.W., Reber, H.A., Hines, O.J., Eibl, G., 2008. Expression analysis of the prostaglandin E2 production pathway in human pancreatic cancers. Pancreas 37, 121–127. https://doi.org/10.1097/MPA.0B013E31816618BA.

Hawcroft, G., Ko, C.W.S., Hull, M.A., 2006. Prostaglandin E2-EP4 receptor signalling promotes tumorigenic behaviour of HT-29 human colorectal cancer cells. Oncogene 21 26, 3006–3019. https://doi.org/10.1038/sj.onc.1210113.

Ito, M., Wang, Q., Hao, D., Sawada, H., Huang, B., Guo, L., Daugherty, A., Li, X.A., 2021. Ultrasound monitoring of thymus involution in septic mice. Ultrasound Med. Biol. 47, 769–776. https://doi.org/10.1016/J.ULTRASMEDBIO.2020.11.031.

Johnson, A.M.F., Costanzo, A., Gareau, M.G., Armando, A.M., Quehenberger, O., Jameson, J.M., Olefsky, J.M., 2015. High fat diet causes depletion of intestinal eosinophils associated with intestinal permeability. PLoS One 10, e0122195.

Karpisheh, V., Nikkhoo, A., Hojjat-Farsangi, M., Namdar, A., Azizi, G., Ghalamfarsa, G., Sabz, G., Yousefi, M., Yousefi, B., Jadidi-Niaragh, F., 2019. Prostaglandin E2 as a potent therapeutic target for treatment of colon cancer. Prostaglandins Other Lipid Mediat. 144, 106338. https://doi.org/10.1016/J.PROSTAGLANDINS.2019.106338.

Karpisheh, V., Joshi, N., Zekiy, A.O., Beyzai, B., Hojjat-Farsangi, M., Namdar, A., Edalati, M., Jadidi-Niaragh, F., 2020. EP4 receptor as a novel promising therapeutic target in colon cancer. Pathol. Res. Pract. 216, 153247. https://doi.org/10.1016/J.PRP.2020.153247.

Kawamori, T., Kitamura, T., Watanabe, K., Uchiya, N., Maruyama, T., Narumiya, S., Sugimura, T., Wakabayashi, K., 2005. Prostaglandin E receptor subtype EP 1 deficiency inhibits colon cancer development. Carcinogenesis 26, 353–357. https://doi.org/10.1093/CARCIN/BGH322.

Keenan, B.P., Saenger, Y., Kafrouni, M.I., Leubner, A., Lauer, P., Maitra, A., Rucki, A.A., Gunderson, A.J., Coussens, L.M., Brockstedt, D.G., Dubensky, T.W., Hassan, R., Armstrong, T.D., Jaffee, E.M., 2014. A listeria vaccine and depletion of T-regulatory cells activate immunity against early stage pancreatic intraepithelial neoplasms and prolong survival of mice. Gastroenterology 146, 1784–1794.e6. https://doi.org/10.1053/J.GASTRO.2014.02.055.

Keith, R.L., Geraci, M.W., Nana-Sinkam, S.P., Breyer, R.M., Hudish, T.M., Meyer, A.M., Malkinson, A.M., Dwyer-Nield, L.D., 2006. Prostaglandin E2 receptor subtype 2 (EP2) null mice are protected against murine lung tumorigenesis. Anticancer Res 26, 2857–2861.

Klein, G.L., Petschow, B.W., Shaw, A.L., Weaver, E., 2013. Gut barrier dysfunction and microbial translocation in cancer cachexia: a new therapeutic target. Curr. Opin. Support. Palliat. Care 7, 361. https://doi.org/10.1097/SPC.0000000000000017.

Lejeune, M., Leung, P., Beck, P.L., Chadee, K., 2010. Role of EP4 receptor and prostaglandin transporter in prostaglandin E 2-induced alteration in colonic epithelial barrier integrity. Am. J. Physiol. Gastrointest. Liver Physiol. 299, 1097–1105. https://doi.org/10.1152/AJPGI.00280.2010/SUPPL_FILE/LEGENDS.PDF.

Li, X., Holtrop, T., Jansen, F.A.C., Olson, B., Levasseur, P., Zhu, X., Poland, M., Schalwijk, W., Witkamp, R.F., Marks, D.L., van Norren, K., 2022. Lipopolysaccharide-induced hypothalamic inflammation in cancer cachexia-anorexia is amplified by tumour-derived prostaglandin E2. J. Cachexia Sarcopenia Muscle 13, 3014–3027. https://doi.org/10.1002/JCSM.13093.

Lu, Y.C., Yeh, W.C., Ohashi, P.S., 2008. LPS/TLR4 signal transduction pathway. Cytokine 42, 145–151. https://doi.org/10.1016/J.CYTO.2008.01.006.

Markosyan, N., Li, J., Sun, Y.H., Richman, L.P., Lin, J.H., Yan, F., Quinones, L., Sela, Y., Yamazoe, T., Gordon, N., Tobias, J.W., Byrne, K.T., Rech, A.J., Fitz Gerald, G.A., Stanger, B.Z., Vonderheide, R.H., 2019. Tumor cell–intrinsic EPHA2 suppresses antitumor immunity by regulating PTGS2 (COX-2). J. Clin. Invest. 129, 3594–3609. https://doi.org/10.1172/JCI127755.

Markovič, T., Jakopin, Ž., Dolenc, M.S., Mlinarič-Raščan, I., 2017. Structural features of subtype-selective EP receptor modulators. Drug Discov. Today 22, 57–71. https://doi.org/10.1016/J.DRUDIS.2016.08.003.

Michaelis, K.A., Zhu, X., Burfeind, K.G., Krasnow, S.M., Levasseur, P.R., Morgan, T.K., Marks, D.L., 2017. Establishment and characterization of a novel murine model of pancreatic cancer cachexia. J. Cachexia. Sarcopenia Muscle 8, 824–838. https://doi.org/10.1002/JCSM.12225.

Millett, C.E., Phillips, B.E., Saunders, E.F.H., 2019. The sex-specific effects of LPS on depressive-like behavior and oxidative stress in the hippocampus of the mouse. Neuroscience 399, 77–88. https://doi.org/10.1016/J.NEUROSCIENCE.2018.12.008.

Mo, C., Zhao, R., Vallejo, J., Igwe, O., Bonewald, L., Wetmore, L., Brotto, M., 2015. Prostaglandin E2 promotes proliferation of skeletal muscle myoblasts via EP4 receptor activation. Cell Cycle 14, 1507–1516. https://doi.org/10.1080/15384101.2015.1026520.

Munford, R.S., 2016. Endotoxemia—menace, marker, or mistake? J. Leukoc. Biol. 100, 687–698. https://doi.org/10.1189/jlb.3RU0316-151R.

Olson, B., Zhu, X., Norgard, M.A., Levasseur, P.R., Butler, J.T., Buenafe, A., Burfeind, K. G., Michaelis, K.A., Pelz, K.R., Mendez, H., Edwards, J., Krasnow, S.M., Grossberg, A. J., Marks, D.L., 2021. Lipocalin 2 mediates appetite suppression during pancreatic cancer cachexia. Nat. Commun. 1 12, 1–15. https://doi.org/10.1038/s41467-021-22361-3.

Peppler, W.T., Anderson, Z.G., Sutton, C.D., Rector, R.S., Wright, D.C., 2016. Voluntary wheel running attenuates lipopolysaccharide-induced liver inflammation in mice. Am. J. Physiol. Regul. Integr. Comp. Physiol. 310, R934–R942. https://doi.org/10.1152/AJPREGU.00497.2015/ASSET/IMAGES/LARGE/ZH60071689740007.JPEG.

PGE2 Produced by Lung Cancer Suppresses Immune Function Through T-regulatory Cells and can be Blocked by the COX2 Inhibitor Celebrex, 2005. Cancer Biol Ther 4. https://doi.org/10.4161/CBT.4.8.2034.

Pochard, C., Gonzales, J., Bessard, A., Mahe, M.M., Bourreille, A., Cenac, N., Jarry, A., Coron, E., Podevin, J., Meurette, G., Neunlist, M., Rolli-Derkinderen, M., 2021. PGI2 inhibits intestinal epithelial permeability and apoptosis to alleviate colitis. Cell. Mol. Gastroenterol. Hepatol. 12, 1037–1060. https://doi.org/10.1016/J.JCMGH.2021.05.001.

Pyter, L.M., El Mouatassim Bih, S., Sattar, H., Prendergast, B.J., 2014. Peripheral tumors alter neuroinflammatory responses to lipopolysaccharide in female rats. Brain Res. 1552, 55–63. https://doi.org/10.1016/J.BRAINRES.2014.01.012.

Rigas, B., Goldman, I.S., Levine, L., 1993. Altered eicosanoid levels in human colon cancer. J. Lab. Clin. Med. 122, 518–523. https://doi.org/10.5555/URI:PII:002221439390010V.

Roy, S., Trinchieri, G., 2017. Microbiota: a key orchestrator of cancer therapy. Nat. Rev. Cancer 17 (5), 271–285. https://doi.org/10.1038/nrc.2017.13.

Ryan, J.L., Carroll, J.K., Ryan, E.P., Mustian, K.M., Fiscella, K., Morrow, G.R., 2007. Mechanisms of cancer-related fatigue. Oncologist 12, 22–34. https://doi.org/10.1634/THEONCOLOGIST.12-S1-22.

Schjerning, A.M., McGettigan, P., Gislason, G., 2020. Cardiovascular effects and safety of (non-aspirin) NSAIDs. Nature Rev. Card. 9 (17), 574–584. https://doi.org/10.1038/s41569-020-0366-z.

Shabab, T., Khanabdali, R., Zorofchian Moghadamtousi, S., Abdul Kadir, H., Mohan, G., 2017. Neuroinflammation pathways: a general review. Int. J. Neurosci. 127, 624–633. https://doi.org/10.1080/00207454.2016.1212854.

Shimonty, A., Bonewald, L.F., Pin, F., 2023. Role of the osteocyte in musculoskeletal disease. Curr. Osteoporos. Rep. 21, 303–310. https://doi.org/10.1007/S11914-023-00788-5/FIGURES/1.

Swanson, L., Katkar, G.D., Tam, J., Pranadinata, R.F., Chareddy, Y., Coates, J., Anandachar, M.S., Castillo, V., Olson, J., Nizet, V., Kufareva, I., Das, S., Ghosh, P., 2020. TLR4 signaling and macrophage inflammatory responses are dampened by GIV/Girdin. PNAS 117, 26895–26906. https://doi.org/10.1073/PNAS.2011667117/SUPPL_FILE/PNAS.2011667117.SAPP.PDF.

Twyman-Saint Victor, C., Rech, A.J., Maity, A., Rengan, R., Pauken, K.E., Stelekati, E., Benci, J.L., Xu, B., Dada, H., Odorizzi, P.M., Herati, R.S., Mansfield, K.D., Patsch, D., Amaravadi, R.K., Schuchter, L.M., Ishwaran, H., Mick, R., Pryma, D.A., Xu, X., Feldman, M.D., Gangadhar, T.C., Hahn, S.M., Wherry, E.J., Vonderheide, R.H., Minn, A.J., 2015. Radiation and dual checkpoint blockade activate non-redundant immune mechanisms in cancer. Nature 520, 373–377. https://doi.org/10.1038/nature14292, 7547.

Valdés-Ferrada, J., Muñoz-Durango, N., Pérez-Sepulveda, A., Muñiz, S., Coronado-Arrázola, I., Acevedo, F., Soto, J.A., Bueno, S.M., Sánchez, C., Kalergis, A.M., 2020. Peripheral blood classical monocytes and plasma interleukin 10 are associated to neoadjuvant chemotherapy response in breast cancer patients. Front. Immunol. 11, 528752. https://doi.org/10.3389/FIMMU.2020.01413/BIBTEX.

van Dierendonck, X.A.M.H., Vrieling, F., Smeehuijzen, L., Deng, L., Boogaard, J.P., Croes, C.A., Temmerman, L., Wetzels, S., Biessen, E., Kersten, S., Stienstra, R., 2022. Triglyceride breakdown from lipid droplets regulates the inflammatory response in macrophages. PNAS 119. https://doi.org/10.1073/PNAS.2114739119/-/DCSUPPLEMENTAL.

Van Norren, K., Dwarkasing, J.T., Witkamp, R.F., 2017. The role of hypothalamic inflammation, the hypothalamic-pituitary-adrenal axis and serotonin in the cancer anorexia-cachexia syndrome. Curr. Opin. Clin. Nutr. Metab. Care 20, 396–401. https://doi.org/10.1097/MCO.0000000000000401.

Wang, D., Dubois, R.N., 2006. Prostaglandins and cancer. Gut 55, 115–122. https://doi.org/10.1136/GUT.2004.047100.

Witkamp, R.F., van Norren, K., 2018. Let thy food be thy medicine….when possible. Eur. J. Pharmacol. 836, 102–114. https://doi.org/10.1016/J.EJPHAR.2018.06.026.

Zhang, G., Li, J., Purkayastha, S., Tang, Y., Zhang, H., Yin, Y., Li, B., Liu, G., Cai, D., 2013. Hypothalamic programming of systemic ageing involving IKK-β, NF-κB and GnRH. Nature 497, 211–216. https://doi.org/10.1038/nature12143, 7448.

Zhang, J., Rivest, S., 2000. A functional analysis of EP4 receptor-expressing neurons in mediating the action of prostaglandin E2 within specific nuclei of the brain in response to circulating interleukin-1β. J. Neurochem. 74, 2134–2145. https://doi.org/10.1046/J.1471-4159.2000.0742134.X.

Zhang, X., Zhang, G., Zhang, H., Karin, M., Bai, H., Cai, D., 2008. Hypothalamic IKKβ/NF-κB and ER Stress Link Overnutrition to Energy Imbalance and Obesity. Cell 135, 61–73. https://doi.org/10.1016/J.CELL.2008.07.043.

Zhao, Z., Ukidve, A., Kim, J., Mitragotri, S., 2020. Targeting strategies for tissue-specific drug delivery. Cell 181, 151–167. https://doi.org/10.1016/J.CELL.2020.02.001.

Zheng, Y., Comaills, V., Burr, R., Boulay, G., Miyamoto, D.T., Wittner, B.S., Emmons, E., Sil, S., Koulopoulos, M.W., Broderick, K.T., Tai, E., Rengarajan, S., Kulkarni, A.S., Shioda, T., Wu, C.L., Ramaswamy, S., Ting, D.T., Toner, M., Rivera, M.N., Maheswaran, S., Haber, D.A., 2019. COX-2 mediates tumor-stromal prolactin signaling to initiate tumorigenesis. PNAS 116, 5223–5232. https://doi.org/10.1073/PNAS.1819303116/SUPPL_FILE/PNAS.1819303116.SD01.XLSX.

Zhou, C., Wu, X.R., Liu, H.S., Liu, X.H., Liu, G.H., Zheng, X.B., Hu, T., Liang, Z.X., He, X.W., Wu, X.J., Smith, L.C., Zhang, Y., Lan, P., 2020. Immunomodulatory effect of urine-derived stem cells on inflammatory bowel diseases via downregulating Th1/Th17 immune responses in a PGE2-dependent manner. J. Crohns Colitis 14, 654–668. https://doi.org/10.1093/ECCO-JCC/JJZ200.